CHAPTER 2: NORMAL CONDUCTING RF INJECTORS

DAVID H. DOWELL

SLAC National Accelerator Laboratory

Menlo Park, CA 94025-7015

Keywords

RF Cavity, Pillbox Cavity, Reentrant Cavity, Racetrack Cavity, Side Coupling, Thermal Management, Emittance Compensation, Wakefield, L-band Gun, S-band Gun, 144 MHz Gun, 1.3 GHz Gun, 433 MHz Gun, 700 MHz Gun, 187 MHz Gun

Abstract

This chapter provides engineering details for normal conducting RF (NCRF) photoinjectors. The basic gun design consists of a conducting cavity shaped to resonate at a desired RF frequency with a port for coupling RF power into the cavity. The two cavity shapes commonly used are pillbox and reentrant. And the two basic coupling schemes to pulse heating used are side-coupled and coaxial coupling. Various technical aspects of these four options in a gun design are discussed in some detail. The few sections describe the topics of the gun's thermodynamics related to pulse heating in a low duty factor gun and average power thermal management in a CW gun. The RF field mode purity and spatial linearity are discussed and the effect on beam quality is quantified. In addition to the gun, the emittance compensation solenoid, bucking coil and diagnostics after the gun are described. Engineering details of beamline components which minimize the emittance growth due to wakefields are presented. The chapter ends with descriptions of photoinjectors which have been built and successfully operated since 1985, when the NCRF gun was invented.

2.1 INTRODUCTION

The need for high brightness electron beams has driven the development of normal conducting RF (NCRF) gun theory and practice. The combination of high accelerating field and the fast switching of photoemission have made these high quality beams possible. In addition, emittance compensation has been shown to be a powerful technique for eliminating the emittance from linear space charge forces. This rapid progress in the electron source technology was driven by the invention of applications, such as the free electron laser, Compton sources and ultra fast electron diffraction. This chapter describes the current state-of-the-art technology for the two classes of NCRF guns: 1) High gradient guns operating at low duty factor, and 2) lower gradient, high duty factor guns. Here, high gradient implies 100 MV m^{-1} or more cathode field and high duty fact means greater than ~10%.

NCRF guns operations span a broad range of RF frequencies ranging from 144 MHz to 30 GHz. Table **2.1** compares different NCRF guns and various properties each have, such as their operating RF frequency, peak cathode fields and duty factors. In general, the higher the duty factor, the lower the RF frequency. On the other hand, the higher frequency guns are capable of much higher peak cathode fields and hence brighter beams.

The peak field and average power of NCRF guns are commonly limited by field breakdown, pulsed heating and average power dissipation. Since the beam quality improves with higher cathode field, NCRF guns operate at the highest possible field strengths.

The RF frequency dependence of the limiting field is given by the Kilpatrick criterion [2.1], [2.2].

$$f_{RF}\,[\text{MHz}] = 1.64\,E_K^2 \exp\left(\frac{-8.5}{E_K}\right) \tag{2.1}$$

where E_K is the Kilpatrick criterion peak field in MV m^{-1}. Figure **2.1** is a plot of the Kilpatrick criterion field versus the RF frequency. The peak cathode fields which guns have achieved are plotted versus their RF frequency in the same graph in Figure **2.1**. The operational gun fields are seen to be approximately a factor of two higher than the Kilpatrick limit above 1 GHz.

RF Frequency Cathode Cavity Shape [Reference]	**Peak Cathode Field [MV/m]**	**Pulse Format**		
		Macropulse Frequency	**Micropulse Frequency**	**Macropulse Length**
144 MHz Reentrant [2.3]	25	10, 20 Hz	14.4 MHz	200 μs
188 MHz Reentrant [2.4]	20	Continuous Wave	1 MHz	(CW)
433 MHz Reentrant [2.5]	25	30 Hz	27 MHz	8300 μs
800 MHz Pillbox [2.6]	5	CW	800 MHz	CW
1.3 GHz Pillbox [2.7], [2.8]	40, 60	10	42 MHz	100 μs
2.856 GHz Pillbox [2.9]	120	120 Hz	single bunch at 120 Hz	2 μs
12 GHz Pillbox [2.10]	200	120 Hz	120 Hz	10 ns
17 GHz Pillbox [2.11]	150	10 Hz	10 Hz	100 ns

Table 2.1. Properties of NCRF guns operating from 144 MHz to 17 GHz.

Dark current is another phenomenon which limits the field strength in guns and accelerators. It occurs at high surface field strength and electrons are produced by field emission from small imperfections in the surface or from particulates on the surface. Since the electrons are emitted at the high field portion of every RF period, this is a serious issue especially for long pulse, high duty factor guns. Besides fabricating a smooth surface, it is also important to clean all RF surfaces of small dust particles. This is an important issue in superconducting RF structures where the technique of high-pressure water rinsing is used. However, recent work shows that dry-ice cleaning is effective at removing hydrocarbons and particles without leaving the surface wet. [2.12] An impressive factor of 10 reduction in the dark current emission has been observed in the PITZ L-band NCRF gun. [2.13]

Since the beam needs to be rapidly accelerated from the cathode, it is standard for RF guns to use the standing wave TM_{011} longitudinal electric mode as given by Equ. 1.8 through Equ. 1.10 in Chapter 1. The TM_{011} mode is called the π-mode because of the 180˚ phase shift between adjacent cells. A gun has as many

longitudinal modes as cells even if they are partial cells, for example, the 1.6-cell gun has 0- and π-modes. Because each mode will have a different spatial shape and RF frequency than the π-mode, these other modes can dynamically unbalance the gun fields and introduce additional emittance. This effect can be both detrimental and beneficial. For example, the introduction of a 3rd-harmonic to the fundamental RF field can both eliminate the 2nd-order RF emittance, as well as straighten the electron energy-time correlation in longitudinal phase space. The use of other harmonic TE modes may provide additional RF focusing, reducing the need for a magnetic solenoid. Details of these modes are discussed later in this chapter.

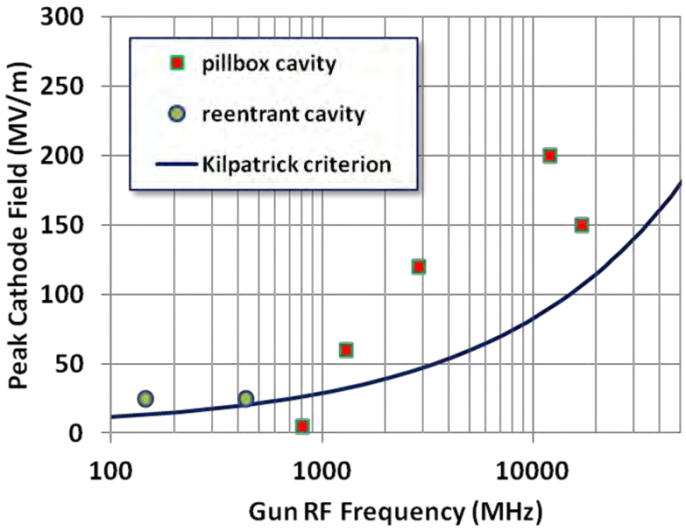

Figure 2.1. Comparison of the frequency dependence of peak cathode fields achieved in operating NCRF guns with the Kilpatrick criterion.

As discussed in Section 1.3.1, there are two basic interior shapes for RF guns: Pillbox and reentrant. These shapes are shown in Figure 1.5 of Chapter 1 and in Figure **2.2**. The pillbox cavity is relatively easy to fabricate, can operate at high electric fields for high RF frequencies and has less radial field distortion compared to the reentrant cavity. The reentrant shape has high shunt impedance, but larger non-linear radial fields. Generally, the pillbox is used in low duty factor guns which run at very high peak powers to produce high cathode field. The reentrant shape is used in high duty factor guns, since it produces higher fields per megawatt of RF power and has a large surface area for cooling.

This chapter ends with sections describing the two basic types of NCRF guns in terms of their duty factor, low or high. For the purposes of this discussion, we define high duty factor as a tens of percent to CW and low duty is everything lower. In general, high duty factor guns are used in Energy Recovered Linacs (ERLs) which operate in CW modes, while low duty factor guns are used for single pass linacs. The last sections of this chapter will describe the common features of these two operating regimes and provide examples of historical and current injector technology. The discussion on beam optics and emittance preservation is applicable to both gun types.

2.2 GUN CAVITY SHAPE AND RF COUPLING SCHEMES

2.2.1 Pillbox and Reentrant Cavity Shapes

As described in Chapter 1, guns are designed to have either a pillbox cavity shape or reentrant nose cones and elliptical side walls. These two shapes are shown in Figure **2.2**. Reentrant cavities tend have larger shunt impedances, and therefore require less RF power. The larger area of the reentrant nose cone improves the average power dissipation of the gun and is often used in high average power guns. The dissipated power of

a cavity is usually the main factor limiting its duty factor. The disadvantages of the reentrant cavity include a more difficult shape to cool and fabricate, especially at higher RF frequencies. In addition, the reentrant shape produces greater non-linear radial fields compared to the pillbox. Generally, the long "tunnel" between cavity nose cones isolates the RF between cells which then requires a separate RF power coupler for each cell as illustrated in the right portion of Figure **2.2**. The power feed for each cell has its RF phase length adjusted to account for the electron's travel time in the relatively long drift length of the tunnel. For this reason, guns using a reentrant shape are configured as either an integrated pair of independently powered reentrant cells or a reentrant cathode cell followed by pillbox cells with a single RF coupling. The typical pillbox shaped cavity consists of closely spaced cells with intervening holes, or irises. These irises are designed to be large enough to allow the coupling of the RF power between cells. This greatly simplifies the waveguide design of the pillbox gun since it needs RF power fed to only one cell. A multi-cell gun using both cell types has been proposed; although in that design, the power is fed to each cell [2.14].

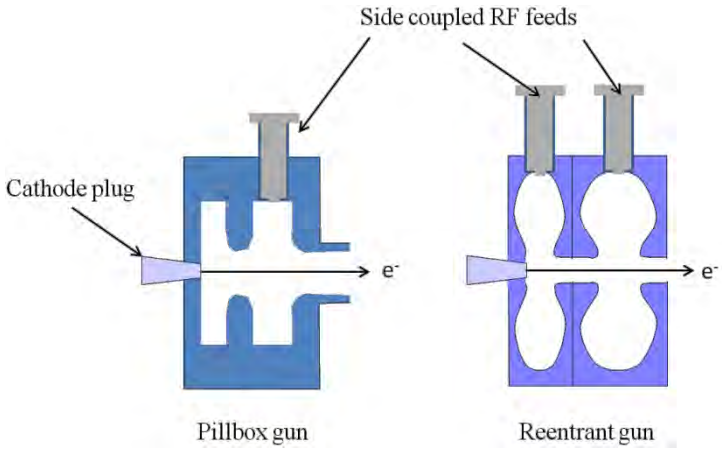

Figure 2.2. Comparison of pillbox (left) and reentrant (right) cavity shapes for gun cavities. Because the pillbox cells are strongly coupled they can be powered by a RF feed on just one of the cells. For the reentrant shape the cell-to-cell coupling is small and an RF feed is needed on each cell.

The RF power, P, it takes to accelerate electrons to an voltage gain of V_0 is

$$P = \frac{V_0^2}{r_{shunt}} \tag{2.2}$$

Here, the gun is considered to be a load with impedance r_{shunt}.

The RF quality factor, Q, is defined as the ratio of the stored RF energy to the averaged dissipated energy over one RF cycle. The Q for cavities with the rotational symmetric TM_{nm0} modes is [2.15]

$$Q = \frac{\mu_0}{\mu_c}\left(\frac{V}{S\delta_{skin}}\right) * \text{(geometric factor); where } \delta_{skin} = \sqrt{\frac{2}{\mu_0 \omega_{RF} \sigma_{wall}}} \tag{2.3}$$

where V is the cavity volume, S is its surface area, and δ_{skin} is the RF skin depth, where σ_{wall} is the conductivity of the cavity walls and ω_{RF} is the RF frequency. The magnetic permeability of the vacuum and the cavity wall conductor are μ_0 and μ_c, respectively. The geometric factor is of order unity for a wide range of cavity aspect ratios and is approximately the same for pillbox and reentrant cavities excited by the same RF mode. The cavity Q can be maximized by increasing the cavity volume while minimizing the surface

area. This accounts for the nearly circular shape of reentrant cavities, giving them a larger ratio of volume to surface area than the pillbox. The peak surface field can be as much as 6X larger at the nosecone of a reentrant cavity producing a higher axial field than the pillbox for the same RF power.

Given these advantages, one may ask why all guns aren't built with reentrant shapes. Referring back to Figure **2.1**, the answer lies with the Kilpatrick criterion. Above ~1 GHz, the achieved peak cathode field is limited by RF breakdown of the cavity surfaces rather than by limitations of the power source. The observed fields are all approximately twice the Kilpatrick criterion for these few gigahertz RF frequencies. At these frequencies, the reentrant would breakdown at the same RF field as the pillbox cavity, although using a reentrant shape would require less RF power to attain the same accelerating field. However, there is a loss of energy gain per physical length since there is no acceleration in the long tunnels between reentrant cavities. Therefore, for the same gap fields, a pillbox gun will be shorter than a reentrant gun for the same acceleration. Since many guns in this frequency region are pulsed and operate at very low duty factor, power efficiency is not a consideration.

However, below ~1 GHz, the peak surface field achievable is no longer limited by breakdown, but rather by other practical issues, *e.g.*, excessive heating of the RF couplers or limited RF power. At these lower frequencies, the RF coupler can become problematic, thereby presenting a significant engineering challenge. In these cases, the reentrant shape improves the power efficiency while increasing the peak cathode and on axis field. As shown in Figure **2.1**, the peak cathode field of the pillbox gun at 800 MHz is below the breakdown criterion and the reentrant guns at 144 and 433 MHz have operated at or above the limit. Although it is generally more difficult to design and fabricate the reentrant cavity, the large cavity size at the low frequencies eases the engineering and fabrication tolerances as well as presenting different design options and requirements. For example, the large cavity size often requires placing the focusing solenoids inside the nose cones instead of around the outside of the gun. And since many low frequency guns are designed to operate at much higher duty factors, power efficiency is important.

2.2.2 Gun RF Theory

The typical layout of the gun RF power flow is shown in Figure **2.3**. The system consists of a RF source connected with a waveguide to a RF coupler. Depending upon the frequency and power levels the coupler can be an antenna probe, a coaxial line or, as shown in the figure, a side coupled waveguide. The RF source power generates the forward power, P_{fwd}, with some going into the gun, P_{cav}, and some being reflected as reverse power, P_{rev}. The total source power is the sum of the cavity and reverse powers, $P_{fwd} = P_{cav} + P_{rev}$.

The RF power enters the gun cavity through a coupling hole or port with a waveguide-cavity coupling parameter $\beta_{coupler}$ defined as

$$\beta_{coupler} \equiv \frac{P_{external}}{P_{cav}} \tag{2.4}$$

Here, $P_{external}$ is the rate the stored energy in the cavity radiates back into the waveguide when the RF source is turned off. P_{cav} is the steady-state power flowing into the gun. Steady-state is defined as when the fields equilibrate and become time-independent. In steady-state, P_{cav} equals the heat dissipation in the cavity walls and the RF power reflected back to the RF source, P_{rev}. The reverse (a.k.a. reflected) power is given by

$$P_{rev} = P_{fwd}\left(\frac{\beta_{coupler} - 1}{\beta_{coupler} + 1}\right)^2 \tag{2.5}$$

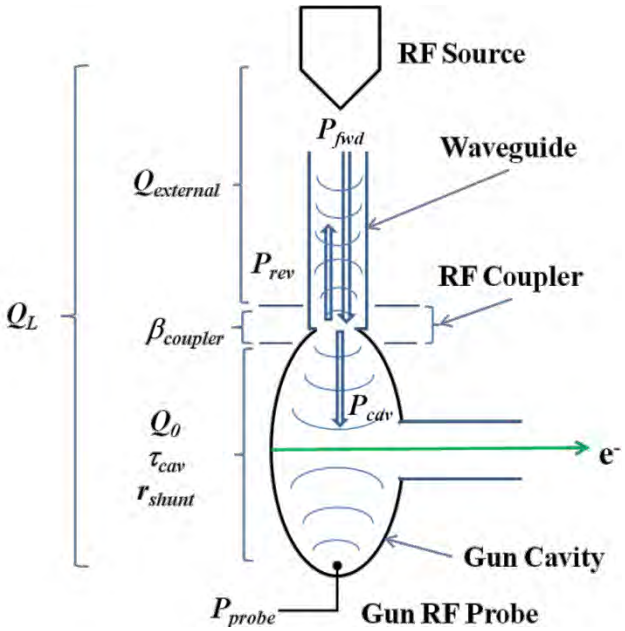

Figure 2.3. Schematic layout of a gun showing the RF power flow and gun and waveguide parameters.

The external and cavity RF powers depend upon the external and cavity quality factors, which are defined as $Q_{external}$ and Q_0 respectively. For a cavity with a stored energy of U and a resonant frequency, ω_0, the external power is given by

$$P_{external} = \frac{\omega_0 U}{Q_{external}} \tag{2.6}$$

and similarly for the steady-state power radiating into the cavity

$$P_{cav} = \frac{\omega_0 U}{Q_0} \tag{2.7}$$

With these definitions, the coupling parameter can be written in terms of the two quality factors

$$\beta_{coupler} = \frac{Q_0}{Q_{external}} \tag{2.8}$$

The quality factor of the entire system is called the loaded-Q, Q_L. In terms of the other quality factors the loaded-Q is given by

$$\frac{1}{Q_L} = \frac{1}{Q_0} + \frac{1}{Q_{external}} \tag{2.9}$$

It can be shown using a resonant circuit model driven at its resonant frequency that the gun's response time to changes in the RF is the 1/e response time, τ_{cav}, given as

$$\tau_{cav} = \frac{2}{\omega_0} \frac{Q_0}{1 + \beta_{coupler}} \tag{2.10}$$

When the fields reach steady-state the cathode field can be related to the forward power using the shunt impedance, the gun effective length, l_{gun}, and the surface field ratio, R_{field}

$$E_{cathode} = R_{field}\left(\frac{\sqrt{P_{fwd}\, r_{shunt}}}{l_{gun}}\right) \tag{2.11}$$

The surface field ratio accounts for any enhancement of the cathode surface compared to the average accelerating field. This enhancement factor is determined by the cavity shape and as discussed earlier is larger for a reentrant cavity than it is for a pillbox. The voltage gain (see Equ. 2.2) is divided by the gun's effective length to give the cathode electric field. For example, the 1.6-cell, S-band gun the shunt impedance is 3.6 MΩ, the effective length is 8.68 cm and the surface field ratio is ~1.8. These parameters can be found for a specific gun design by using a field solving code such as SUPERFISH [2.16].

It is important to stress that the above relations apply only when the gun fields have reached their steady-state values, that is when $t >> \tau_{cav}$. When the RF power is initially turned on there are transients whose time-dependence is determined by the gun's response time often called the cavity fill time. Figure **2.4** shows measurements of the forward, reverse and gun probe powers for an S-band gun being driven by a 1.2 μs long RF pulse. This pulse is just long enough to fill the gun and launch a single electron bunch. This pulse structure minimizes the average power dissipation.

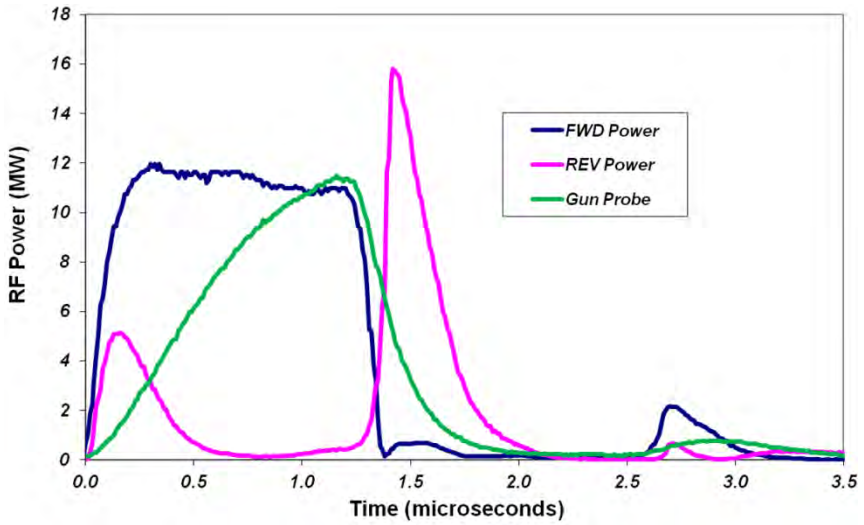

Figure 2.4. RF waveforms measured during high power operation of an S-band gun. The small pulses near 2.7 μs are the reflections of the RF pulse from the klystron.

The behavior of the reverse RF is determined by the voltage reflection coefficient, Γ, defined in terms of the forward and reverse voltages, respectively V_{fwd} and V_{rev} [2.17]

$$\Gamma(t) = \frac{V_{rev}(t)}{V_{fwd}} = (1 - e^{-t/\tau_{cav}})\,\frac{2\beta_{coupler}}{1+\beta_{coupler}} - 1 \tag{2.12}$$

This reflection coefficient produces a time-dependent reflection of power back toward the RF source given by the forward power times the voltage reflection coefficient squared,

$$P_{rev}(t) = P_{fwd}\,\Gamma(t)^2 \tag{2.13}$$

Consider Equ. 2.12 and Equ.2.13 at short and long times. At the start of the RF pulse, $t = 0$, all the forward power is reflected independent of the coupling coefficient. For times long compared to τ_{cav} the system is in steady-state and the reflected power is given by Equ. 2.5 which has three regimes of interest. If $\beta_{coupler} < 1$, then the system is said to be undercoupled and there is always power reflected by the coupler. For $\beta_{coupler} = 1$, the system is critically coupled and the reflection becomes zero after several cavity times. If $\beta_{coupler} > 1$, then the system is overcoupled and after some time the reverse power goes first to zero and then at longer times increases again to the value given by Equ. 2.5. The measurements shown in Figure **2.4** are for an overcoupled gun where the reverse power becomes zero near 0.7 μs and then rises to its steady-state value.

At the end of the RF pulse, the forward power becomes zero and the reverse power immediately rises as the cavity's stored energy radiates back into the waveguide. The ratio of the radiated power in the reverse wave to the cavity power is

$$\frac{P_{rad}}{P_{cav}} = \left(\frac{2\beta_{coupler}}{1+\beta_{coupler}}\right)^2 (1 - e^{-t/\tau_{cav}})^2 \tag{2.14}$$

For the S-band (2.856 GHz) gun data shown in Figure **2.4** the coupling coefficient is 2 and the Q_0 is 13 900, thus cavity time constant as 0.516 μs. Using these values in Equ. 2.14 gives $P_{rad}\, P_{cav}^{-1} = 1.45$ when the pulse ends at $t = 1.2$ μs. Since, at the end of the pulse $P_{fwd} \approx P_{cav}$, one sees in Figure **2.4** that the reverse power jumps to 1.4X P_{fwd} in agreement with Equ. 2.14.

The reverse power reflects back and forth between the gun and the RF source producing distortions in $P_{external}$ and P_{cav}. These reflections can result in large variations in the phase and amplitude during the RF macropulse, and under some conditions constructively interfere with the forward RF wave to create locations of high field which electrically breakdown. In addition, a strong reflection back into the klystron can disrupt its output. For these reasons, it is usually necessary to protect the RF source from the reflected power. This can be done using a device called a RF isolator or a very long waveguide, in which the RF pulse ends before the reflection can travel back to the RF source. The topic of RF isolation is discussed again later in this chapter.

2.2.3 RF Coupling Schemes

There are three geometries which are commonly used for coupling the gun to the waveguide. These are: 1) Waveguide coupled to the cavity side wall; 2) coaxial RF feed using a door-knob mode transformer; and, 3) coaxial transmission cable and inductive loop coupling. The engineering details of RF fundamental power-couplers are discussed in Chapter 10, Section 10.4.

The most commonly used coupling is waveguide side coupling which has been used over the full frequency range RF guns have operated, *i.e.*, from 144 MHz to 17 GHz. A disadvantage of side coupling is that it induces a radial asymmetry in the axial RF fields which can increase the beam emittance. The RF field asymmetries can be minimized by using symmetric ports and a racetrack shape for the coupled cell as shown in Figure **2.5(a)**. The dipole and quadrupole field distortions on the beam axis are corrected by using dual feed ports and a racetrack cavity shape. The drawing shows the gun with both dual feeds and a horizontally wider coupler cell, a.k.a. a racetrack shape, to produce rotation symmetric RF fields [2.18].

The second coupler geometry is a coaxial coupler designed to maintain full rotational symmetry and has been successfully used in guns at 1.3 and 3 GHz. The design for an L-band gun is shown in Figure **2.5(b)**.

The coaxial coupler maintains rotation symmetry by having no asymmetric penetrations into the gun cavities. This design requires transforming the waveguide mode into a radial coaxial mode with a "door-knob" mode converter. Chapter 10, Section 10.4 provides more engineering details of the waveguide vacuum windows, low voltage breakdown (multipacting) and other practical considerations for the coaxial waveguide coupler design.

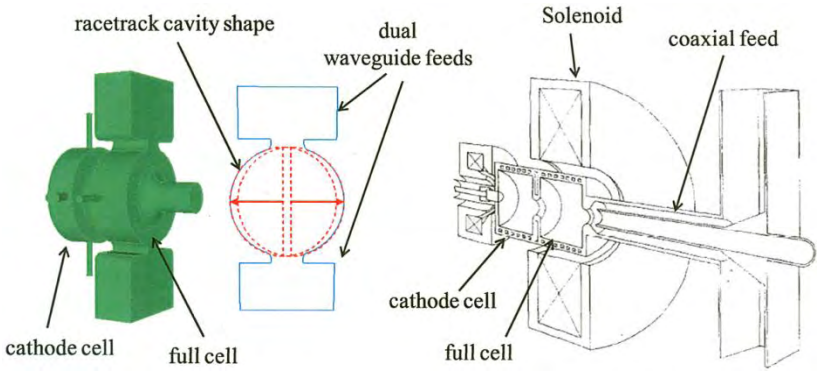

Figure 2.5. The side-coupled (a) and coaxial (b) feed geometries for symmetrically coupling the RF power into the gun. The solenoids for the side-coupled gun are not shown. [2.19] [[2.9]; Adapted under Creative Common Attribution 3.0 License (www.creativecommons.org/licenses/by/3.0/us/) at www.JACoW.org.] [Adapted from [2.20], with permission from Elsevier.]

The third coupler geometry consists of a coaxial cable connected to a loop antenna in the cavity. This approach is appropriate for low RF frequencies and is limited to lower levels of power than the other two methods. An example of coaxial lines feeding dual RF loop couplers in a 188 MHz gun is shown in Figure **2.6**. In this single cavity gun two couplers transmit RF into a cavity. Two loop antennae are used because the required power is more than a single loop can handle. Since the couplers are located far from the beam axis, they have negligible influence on the RF field symmetry.

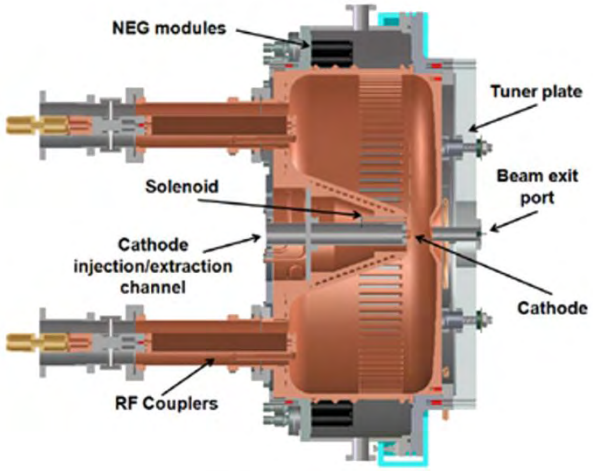

Figure 2.6. Coaxial cable feed and loop coupling for the LBNL 188 MHz gun cavity. [[2.21]; Available under Creative Common Attribution 3.0 License (www.creativecommons.org/licenses/by/3.0/us/) at www.JACoW.org.]

2.3 GUN THERMODYNAMICS AND RF POWER SYSTEM

While the gun resonant frequency is determined by the cavity shape, the stability of this frequency and the RF amplitude and phase is determined by the gun temperature. Since it is necessary to operate with a high cathode field, and in some cases high average power, there is significant heating of the cavity walls. This heating is especially problematic around the penetrations for the RF couplers, the RF probes and laser ports.

This heating manifests itself on two separate time scales, pulsed heating and average power heating. Generally, pulsed heating is confined to the cavity surfaces and occurs for RF pulses short compared to the mechanical response time of the cavity material. Average power heating affects the overall temperature of the gun. The RF power and cooling system are responsible for keeping the gun at resonance and stabilizing the phase and amplitude of the fields. This section discusses the gun's thermal design and RF control system.

2.3.1 Thermal Management of High Power RF

RF heating of the gun can be classified by the two time scales of pulsed and average power heating. Pulsed heating occurs during the RF macropulse that can range from sub-microseconds to milliseconds on a time scale which is short compared to the time it takes the material to mechanically expand. Between RF pulses, the heat diffuses away from the thin RF skin depth and the temperature falls until the next RF pulse. Thus, there are rapid cycles of expansion and contraction of the cavity surface. If the thermal stress induced by each RF pulses exceeds the elastic limit of the cavity material, then microcracks will form at the grain boundaries. With continued pulsing of the gun these microcracks can enlarge and propagate ultimately becoming sites for RF breakdown [2.22].

For guns operating in the long macropulse and/or high repetition rate regime, average heating becomes an issue. What is considered high average heating depends upon the RF frequency. The low RF frequency gun can dissipate higher average power than higher frequency guns. This is because the larger surface area reduces the surface power density making cooling easier. For NCRF guns the RF surface resistant will vary as $\sqrt{f_{RF}}$ and an acceptable surface heat density is about 20 W cm^{-2}. At very high average power the cavities will detune and reject the RF power, or if the gun is kept in tune the thermal stresses between different parts of the gun exceed the elastic limit and the mechanical interfaces can become distorted and fail.

RF heating at a penetration occurs where the wall current is deflected around holes and bumps in the cavity walls. These surface deformities locally increase the surface resistance to make hot spots. Since this heating is localized within the skin depth of the surface (a few micrometers), it is difficult to cool, especially for pulsed heating. The pulsed heating around penetrations can be mitigated by reducing the curvature of the surfaces and minimizing the number of penetrations.

The heat load on the gun walls will raise the gun body temperature, causing it to expand and shift the resonant frequency. If the gun is not designed and built with rotational symmetry, then it will flex asymmetrically at the higher operating temperatures and produce asymmetric RF fields which distort the beam. Thermo-mechanical analysis of the design using 3-D codes, such as ANSYS, and 4-D codes, like MAFIA, is an important aspect of most gun studies. Transient and steady-state simulations of the gun body temperature distribution and the mechanical stresses are typically performed.

As first example, we present thermodynamic calculations comparing two S-band (2.856 GHz) gun designs both operating at 4 kW of average power. This average power corresponds to a peak cathode field of 140 MV m^{-1} and a 120 Hz pulse repetition rate with 3 μs long RF pulses. These are the requirements of the gun for an X-ray light source user facility.

We compare the steady-state surface temperature distributions of the BNL/SLAC/UCLA gun (Figure **2.7(a)**) and the LCLS gun (Figure **2.7(b)**) operating at 4 kW average power dissipation. The temperature distribution for the BNL gun indicates the cathode is hot at 90 ˚C. Thus, there will be considerable expansion of the cathode plate relative to the gun body. The heating around the thin edges of

the RF coupling port in the gun of Figure **2.7(a)** produces a peak von Mises stress of 14 kPSI [2.23]. This stress is 3-4X higher than the yield strength for brazed copper. In addition, a calculation of the pulsed heating around the coupler port gives a temperature rise of 137 ˚C per pulse which is 3X the acceptable limit established for X-band (11.8 GHz) structures [2.22]. The maximum heat flux of 70 W cm^{-2} is more than 3X higher than the maximum average heat load of 20 W cm^{-2}. All these results indicate this gun design would have a limited lifetime operating continuous at the required 4 kW average power.

Figure **2.7(b)** shows an upgraded version of the gun which uses a long and wide coupling port for the RF and cooling has been added to the cathode. Temperatures and the mechanical stresses are significantly less in this design. Here, the maximum temperature at the coupler port is 36 ˚C for 4 kW of power dissipation compared to > 90 ˚F at the cathode in the previous design.

The pulse heating of the Z-coupling ports was optimized by increasing the radius of curvature of the edge of the port running the length of the cavity. Computer modeling gives a temperature rise of 42 ˚C at a 140 MV m^{-1} cathode field. This temperature rise is safely below the recommended upper limit of 50 ˚C determined in the X-band cavity studies [2.22].

The results shown in Figure **2.7** are typical are for pillbox guns, but for a reentrant gun the distribution is distinctly different due to the nose cones. The higher cathode and on axis fields are achieved by increasing the current density with the nose cone shape. This higher current density also increases the surface heating in this region. The hotter area is a ring around the nosecone just behind the "nose." A thermal model for a 1 300 MHz L-band gun operating at 5% duty factor gives a temperature rise of 60 ˚C just behind the bulge of the cathode nosecone. The same temperature rise is found around the RF coupler port. The analysis was done for 10 kHz repetition rate, a peak cathode field of 64 MV m^{-1} and an average dissipated power of 29 kW. This design has areas with a peak power density greater than 110 W cm^{-2} [2.6] which are over 5X the 20 W cm^{-2} limit generally used for accelerator cavities.

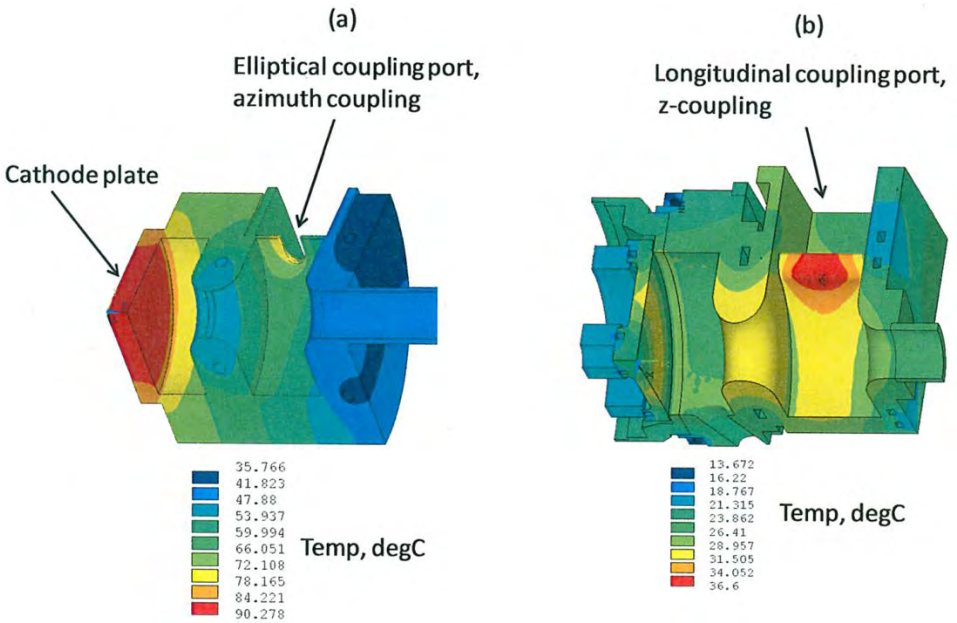

Figure 2.7. a) A ¼ model of the body temperature for the BNL/SLAC/UCLA S-band gun operating at 3.7 kW of average power. [2.24] b) The ¼ model of the Z-coupled LCLS gun showing the steady state temperature distribution for 4 kW of average RF power dissipation. [[2.23]; Adapted under Creative Common Attribution 3.0 License (www.creativecommons.org/licenses/by/3.0/us/) at www.JACoW.org.] [2.19]

The large power dissipation of high duty factor and CW NCRF guns requires careful thermal design of the gun cavities and the RF coupler. A good example of a CW coupler design is that used in the LANL/AES 2.5-cell gun operating at 700 MHz [2.25]. Dual RF feeds are used on the coupling cell to minimize any field asymmetry on the beam axis. The dual feed also allows splitting of the RF power, thereby sharing the heat load between two RF vacuum windows. The cavities are pillbox in shape and use a novel "dog-bone" shape for the RF coupling ports [2.26]. The waveguide transitions are tapered ridges to couple the RF power from the half height waveguide to the coupling ports. The ridge-loaded, tapered waveguide (RLWG) is carefully designed to minimize the reflected RF power as well as multipacting. Multipacting in the RLWG and excessive heating of the coupler holes was observed in CW operation of a Radio Frequency Quadrupole (RFQ) proton accelerator [2.27]. The electron gun was designed with 2-D and 3-D, frequency-domain and time-domain codes [2.28] to avoid these problems.

The dog-bone coupling port consists of two holes connected by a long, narrow slot through a sidewall of the cavity. The hole diameters are equal and adjusted to give the desired coupling coefficient while keeping their area small. The larger the area, the greater the surface current density increases around the hole. The narrow slot minimizes the axial field perturbation and allows cooling channels along its walls. The coupler consists of end holes 4.75 mm in radius at each end of a 5 cm long, 1.788 mm wide slot. The cavity wall thickness at the coupler is 12.7 mm. The coupling coefficient is 1.38 and the external Q is 1 933[2.4]. The gun's Q_0 is 31 800 [2.25]. Enhanced cooling at the edges of the holes is necessary to avoid melting the opposing ends of the holes. [2.27]. Since the wall current dominantly flows parallel to the slot, this geometry only perturbs the wall current where it flows around the holes and thus is where much of the heating occurs. A thermal analysis for 461 kW of forward power shows a power density of 120 W cm^{-2} at the outer edges of the holes.

While the pillbox cavity avoids the hot annulus behind the nose cone, there remains a large heat load of over 100 W cm^{-2} covering large radial patterns upon the cavity walls. This is only slightly lower than the maximum power density of the coupler and produces stresses well above the tolerable yield strength of brazed copper. As a result, this and other high stress designs require the use of a higher yield strength copper-alumina sintered material called GlidCop® [2.29].

2.3.2 The Photoinjector Control System

All NCRF guns require active regulation and monitoring of a multitude of gun parameters, ranging from the RF power to the gun body temperature. A schematic layout of the gun control system is shown in Figure **2.8**. It's built from three basic parts: The sensors and actuators, the process variable database, and the high-level computer applications. The sensor & actuator level includes any feedback or feedforward controls which are either hardwired or embedded in local processors. An example of a hardware controller at the sensor & actuator level would be the fast feedback loop for maintaining the desired RF phase and amplitude during the RF macropulse. The field ϕ-A control box takes the forward- and reverse-RF power signals from the directional coupler along with the cavity RF probe signals and compares them with the desired RF phase and amplitude. All the information used by and varied by the RF field controller is available in the process variable database. High-level applications could change the controller's settings such as the desired RF power and the controller would regulate the RF to that value. In this architecture, the high-speed control is done by fast embedded hardware while the slower feedback and monitoring is done by the high-level applications.

The sensor and actuator signals are stored in a common database and are called "process variables," or PVs, for short. A PV can be a scalar or an array of values. Examples of scalar sensor PVs are the gun body water

temperature and the peak forward klystron power. The digitized waveform of the RF macropulse shape would be an array PV. The PV information in the database is accessible by both the sensor/actuator hardware and the high-level applications. The local controllers continually update the sensor PVs on the database and read the values and status of the actuator PVs set by the high-level applications. The high-level applications monitor the sensor PVs and vary actuator PVs to modify and regulate the overall system.

The cooling system for high power guns can be fairly large and are usually located some large distance from the gun itself. This can make the circulation loop time fairly long compared to the RF power response time, leading to control loop delays and possibly slow and unstable temperature control. This problem is solved by installing a small temperature controlled chiller near the gun.

A small fraction of the water from the main loop is diverted through the chiller which the chiller heats or cools in order provide precise and fast control of the cavity temperature, and hence resonance frequency. The water system regulation needs to be stable and accurate enough to keep the resonance frequency within the control range of the LLRF system. For most cases the water system needs to regulate the gun body temperature with an rms temperature variation of 0.1 ˚C to be within the control range of the LLRF.

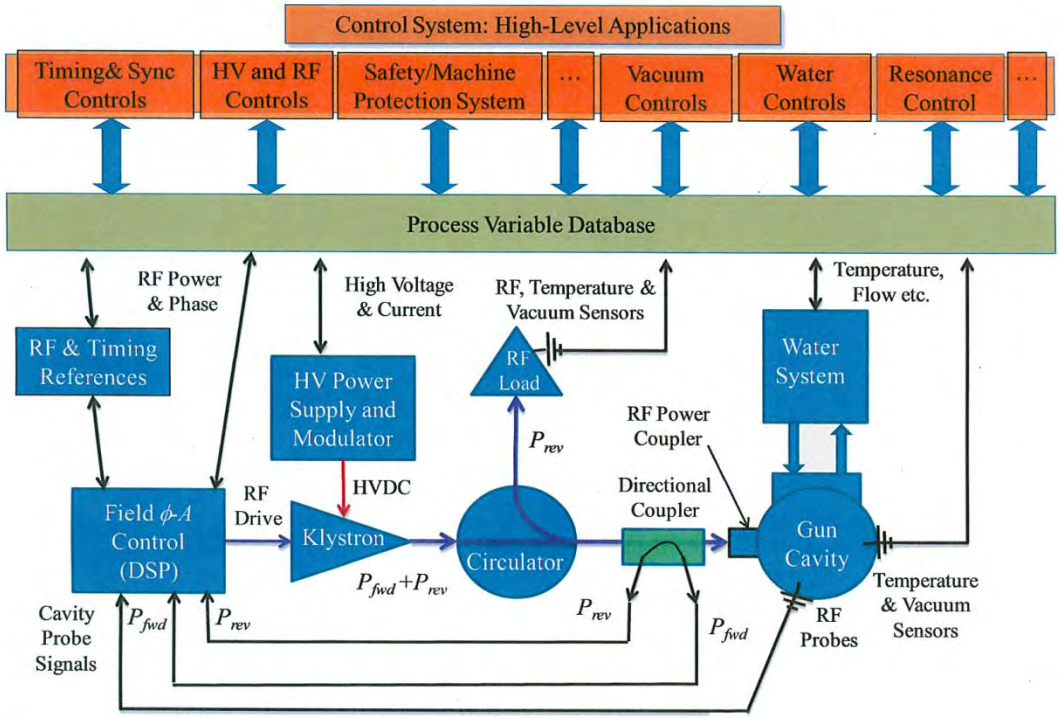

Figure 2.8. Schematic drawing of gun RF and water control systems. The drawing shows the water and resonance controls being connected by an internal control application.

The RF system includes a field phase and amplitude controller which compares signals from a gun cavity probe and a directional coupler with the RF reference to generate the low level drive for the RF amplifier (which is usually a klystron). A directional coupler near the gun coupling port samples a fraction of the forward- and reverse-RF power. The RF power source also requires a high voltage, high current power supply, and pulse modulator, which also requires a feedback circuit for stable operation. As discussed earlier, a large fraction of the RF power is reflected back from the gun at the start and end of the RF pulse and the RF source needs to be protected from these reflections. For short macropulses, the klystron can be isolated by time, that is, by delaying the reflection so it arrives back at the source after the RF macropulse

ends. In practice the reflection is delayed by using a very long waveguide between the klystron and the gun which physically limits its application pulse formats with RF macropulses less than ~2 μs long. The isolation for long macropulses and CW operation uses a device called a three-port circulator which behaves like a RF diode. The circulator shown in Figure **2.8** passes the forward power into the gun, while directing the reflected, reverse power to an impedance matched RF load. RF isolation is discussed with more detail in Chapter 10, Section 10.3.

2.4 RF CAVITY FIELDS AND EMITTANCE

In this section, we discuss the effect the RF field has on the electron beam quality. In Chapter 1, the RF emittance was shown to be solely due to the time dependence of the fields; however, the RF field can also have a spatial variation which can distort the beam. The spatial distribution of the field is determined by the RF-mode being used, details of the cavity shape and the locations of penetrations, such as the RF coupler in the cavity walls. The emittance due to side-coupled RF ports is discussed along with a method for correcting the field asymmetry. It is similarly important to have symmetric RF fields in the first accelerator section after the gun and the racetrack design, for its field correction is also described. Later in this section, the effects of mode purity and the spatial field asymmetries are described.

2.4.1 RF Transverse Fields and Emittance

The RF coupling port can generate an asymmetric field distribution about the beam axis which can distort and reduce the beam quality. The dipole asymmetry can be removed by using a pair of phase and amplitude balanced opposing RF couplers, however, there remains the quadrupole and higher order fields. To aggravate the issue, the large, Z-coupled ports produce larger quadrupole fields than the smaller, oval ports of the BNL/SLAC/UCLA gun. The coupling coefficient for the Z-coupled is 2, and the coupling for the original BNL/SLAC/UCLA gun's oval ports is 1.3.

The RF quadrupole field can be canceled by making the coupler cavity slightly wider in the direction perpendicular to the coupler ports. This is called a racetrack cavity shape and was originally proposed for X-band travelling wave structures [2.30]. The RF quadrupole field introduced by the ports is compensated for by slightly elongating the cell in the direction perpendicular to the coupler ports. The cross section of the coupling cavity shape is shown in Figure **2.9**. In this design, the racetrack shape is formed by two circles whose centers are offset a distance d_{sep}.

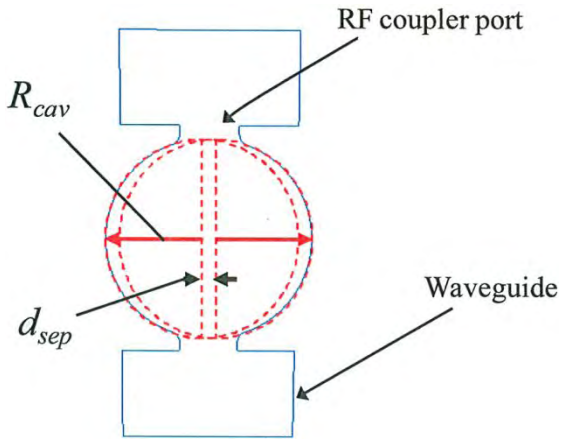

Figure 2.9. Cross-section of the coupling cell for a side-coupled, dual RF feed gun. [[2.9]; Adapted under Creative Common Attribution 3.0 License (www.creativecommons.org/licenses/by/3.0/us/) at www.JACoW.org.]

The radial kick from the quadrupole field is found by integrating electron trajectories through the time-dependent, 3-D cavity fields. The cavity fields are computed using details of the cavity surface shape and penetrations [2.29]. Analysis shows cavities with rotational symmetry behave as time-dependent electric lenses with focal lengths given in Chapter 1, Section 1. Adding opposing side ports for dual RF feeds is effective at eliminating the dipole RF kick, but it introduces a quadrupole field with a thin lens-like kick. Here, the quadrupole kick is defined as the focal length of a thin lens with the same angle change as computed from the 3-D field.

The quadrupole kick or lens strength, $1/f_{rfq}$, is given by

$$\frac{1}{f_{rfq}} = a_q \sin(\phi_{RF}) \tag{2.15}$$

The RF quadrupole focusing strength, $1/f_{rfq}$, has a unit of m^{-1} (or equivalent units would be mR mm^{-1}). If the focal length is in meters, then the focal strength unit is the diopter. The amplitude of the sinusoidal focal strength is a_q and ϕ_{RF} is the RF-bunch phase. Figure **2.10** shows the quadrupole focal strength computed from the 3-D fields for dual RF ports configured with ellipse-shaped, azimuth-coupled ports as shown in Figure **2.7(a)** [2.23]. The lens strength is plotted as a function of the RF phase for d_{sep} = 0, 3.15, 3.56 and 3.40 mm. The plot for d_{sep} = 0 is the case for RF ports (coupling factor of 2) in a round cavity. The quadrupole field is zeroed for d_{sep} = 3.40 mm. Analysis shows the lens strength for the corresponding *Z*-coupled cavity is similar to that of azimuthally coupled cavities provided they have the same RF coupling factor. The peak quadrupole focal strength corresponds to a focal length of 222 mm which is approximately twice the radial RF focal length. See Chapter 1, Section 1.5.1.

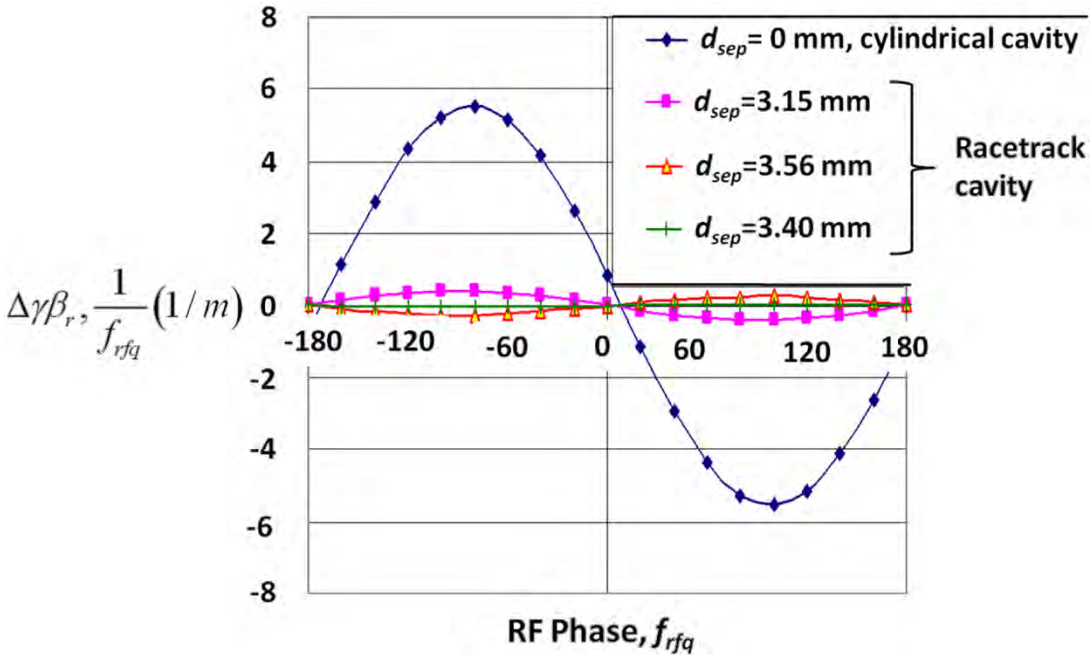

Figure 2.10. The integrated transverse kick (1/m) due to the RF quadrupole field is plotted as a function of the RF phase. The quadrupole field is due to the RF field extending into the dual feed ports. The RF coupling factor is ~2 for both port configurations. RF crest is at zero degrees. The quadrupole lens strength for an elliptical port with its long axis in the azimuth direction as shown in Figure 2.7(a). [[2.23]; Adapted under Creative Common Attribution 3.0 License (www.creativecommons.org/licenses/by/3.0/us/) at www.JACoW.org.]

As described in Chapter 1, a quadrupole field produces emittance effects somewhat different from those for rotational symmetric fields. Similar to the rotational symmetric fields, the time-dependence of the quadrupole field generates a first order projected emittance due to different focusing of each slice. The second order RF projected emittance due to the quadrupole field similarly results from the curvature of the RF waveform. However because the quadrupole field distribution does not have rotational symmetry, the beam's rotation in the solenoid field couples the *xx'* and *yy'* trace spaces. With this coupling the *xx'* phase space correlations with the *yy'* phase space appears to change the 2-D emittances, while the 4-D canonical emittance of would remain constant. The correlations affect both the slice and projected 2-D emittances. The correlated trace space emittance due to an anomalous quadrupole field is described in Chapter 1, Section 1.5.4. The emittance due to the RF quadrupole lens strengths shown in Figure **2.10** is discussed next.

Similar to the derivation for the RF emittance given in Chapter 1, Equ. 1.26, one can write the first-order RF quadrupole emittance as

$$\varepsilon_{rfq}^{(1)} = a_q \, \sigma_x^2 \left| \frac{\mathrm{d}}{\mathrm{d}\phi_{rf}}\left(\frac{1}{f_{rfq}}\right)\right| \sigma_\phi \tag{2.16}$$

The average transverse rms beam size in the quadrupole field region is σ_x and the rms bunch phase length is σ_ϕ in radians. Inserting the relation for the quadrupole lens strength gives

$$\varepsilon_{rfq}^{(1)} = a_q \sigma_x^2 \sigma_\phi \left|\cos(\phi_{rf})\right| \tag{2.17}$$

Similarly the second-order emittance is found to be

$$\varepsilon_{rfq}^{(1)} = \frac{a_q}{\sqrt{2}} \, \sigma_x^2 \sigma_\phi^2 \left|\sin(\phi_{rf})\right| \tag{2.18}$$

Recall that a_q is the amplitude of the sinusoidal quadrupole lens strength versus the RF phase. The graph of the cylindrical cavity quadrupole strength shown in Figure **2.10** indicates a_q (cylindrical, azimuth) = 5.5 m^{-1}.

Adding the first and second order RF quadrupole emittances in quadrature gives the total emittance due to the quadrupole RF field,

$$\varepsilon_{rfq}^{(1+2)} = a_q \sigma_x^2 \sigma_\phi \sqrt{1 - \left(1 - \frac{\sigma_\phi^2}{2}\right) \sin^2(\phi_{rf})} \tag{2.19}$$

Since the asymptotic bunch-RF phase is always within ±20 ˚RF of the RF crest, the emittance in this region is ~0.3-0.4 μm for σ_ϕ = 0.0705 radians (4˚ RF-rms) and a_q = 5.5 m^{-1}. This is all due to the first order quadrupole RF emittance.

Beyond emittance growth in the gun, it is also necessary to study the RF field effects in the first accelerator section (booster) after the gun. Field asymmetries can have a large effect, since the beam energy is still low. As an example, consider the SLAC S-band travelling wave linac after the LCLS gun. Applying the same field analysis as was done for the gun, one finds a similar head-tail, projected emittance. Figure **2.11** shows

the transverse momentum change of the beam as it transits the coupler fields. The inserted drawing shows the dual feed, racetrack coupling cell and its location in front of the first cavities of the linac section. The radius of the port edge should be 1 mm or larger to minimize pulsed heating [2.31].

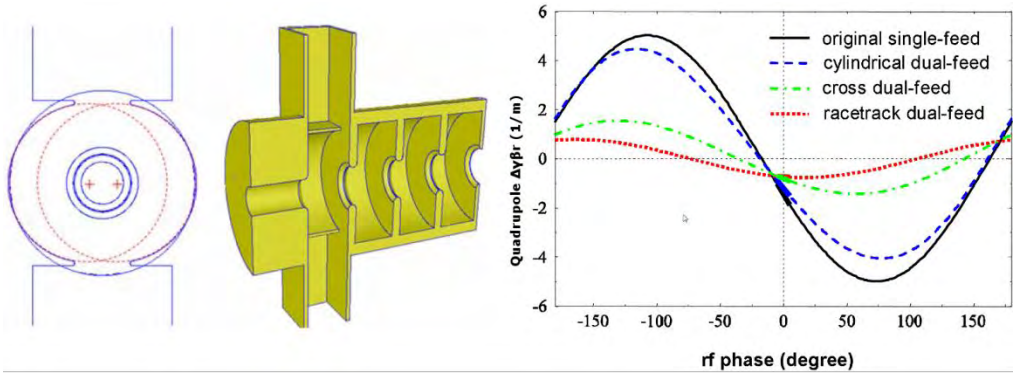

Figure 2.11. Transverse momentum change of the beam after crossing the RF coupler quadrupole field. Beam energy crests at zero ° RF phase. (Left/Middle): Travelling wave S-band linac with a dual feed racetrack RF coupler. The coupling port runs the length of the coupling cell (Z-coupling) and the cavity inside shape is defined by two, offset circles to approximate a "racetrack" shape. [[2.23]; Available under Creative Common Attribution 3.0 License (www.creativecommons.org/licenses/by/3.0/us/) at www.JACoW.org.]

2.4.2 RF Modes and the Emittance

In guns with n coupled cavities there are *n* longitudinal RF modes. Since it's important to excite only the π-mode, the other modes should be several MHz away in resonant frequency. The RF gun is said to have balanced fields if the peak field is the same in all cavities for the π-mode. The field balance is typically measured using Slater's perturbation technique, in which, a small dielectric or metal bead is inserted into the cavity and the resulting change in the RF resonant frequency is measured as a function of the bead's position in the cavity. Taking measurements for the 0- and π-mode resonances as a function of bead position gives the shape of each mode in the gun.

One set-up for performing these measurements is the bead drop technique as shown in Figure **2.12**. In the bead drop technique, the bead is held at the end of a thin surgical string thread and the resonant RF frequency measured for the π- and 0-modes as the bead is lowered to the cathode. In open ended RF structures, the bead is suspended in the middle of the string which is pulled through the structure; this is called the bead pull technique. Dropping the bead is preferred for guns since it measures the field very near the cathode wall without the fields being perturbed by a hole for the string.

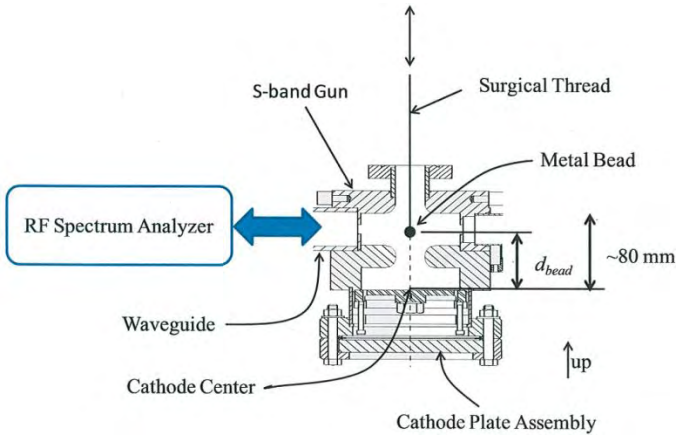

Figure 2.12. Set-up for measuring the field shape using the Slater perturbation method.

Bead-drop measurements for the π- and 0-modes of a 1.6-cell S-band gun are shown in Figure **2.13**. The π-mode, which is the desired accelerating mode of the gun, is seen to be balanced. That is, the electric field at the cathode (bead position = 0 mm) is equal to the peak of the electric field in the full cell. In contrast, the 0-mode shape is quite different and is not balanced between the two cavities.

The measurements shown in Figure **2.13** are performed using a narrow bandwidth (small frequency spread) CW RF source to selectively excite only the 0- or π-mode. However, if the gun is powered by a pulsed RF source both modes can be excited. Consider a 1.6-cell S-band gun with a 3.2 MHz mode separation being powered with a 2 μs long pulse with approximately 300 ns rise time. This fast pulse easily can excite the 0-mode since a ~300 ns rising edge has significant frequency components out to 3 MHz or more around the drive frequency. Measurements of an S-band gun in operation with a 2 μs RF pulse indicate the gun field is oscillating at frequency of the mode separation of 3 MHz and a peak-to-peak amplitude of 3-5%. [2.32]

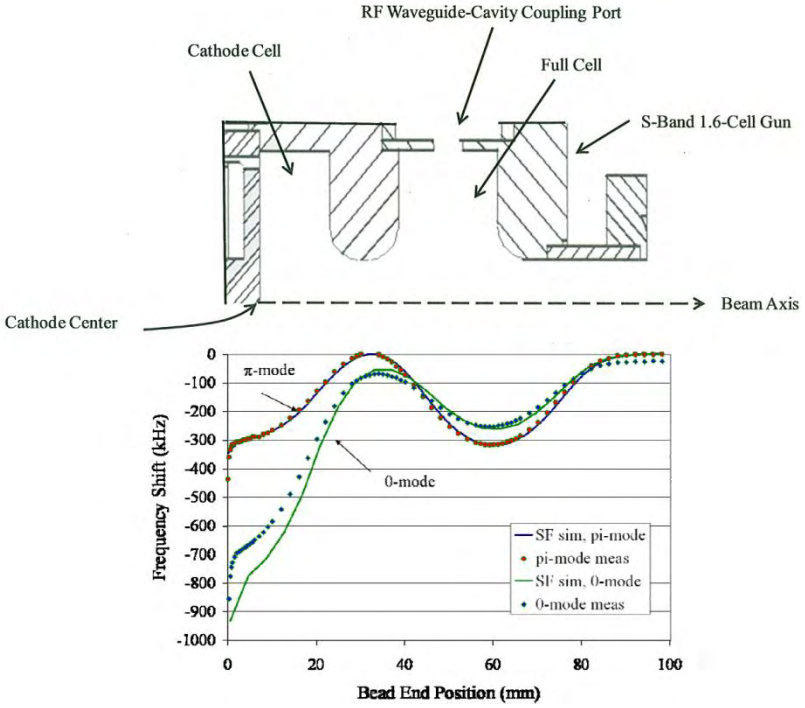

Figure 2.13. Top: Upper half of cross section through a 1.6-cell S-band gun. Bottom: Bead drop measurements of the 0- and π-modes for a 1.6-cell S-band gun as a function of bead position from the cathode. The cathode is located at the 0 mm bead position. Points are the frequency difference between the resonance frequency measured at each bead position minus the resonance frequency when there is no bead in the cavity. The solid curves are a simulation using the SUPERFISH RF code [2.16]. [2.19]

A consequence of exciting both RF modes can be seen in the energy spread and the emittance. Because the field balance requirement for the π-mode is 1-2%, a 3-5% contamination by the 0-mode unbalances the cavity fields and produces a correlated energy along the bunch. Since the energy spread is correlated it can be removed with the high energy linac, however at some energy cost of operating with the beam a few degrees away from the crest of maximum energy gain.

Ignoring longitudinal wakes, there will be a phase shift between maximum energy gain and minimum energy spread. This phase shift gives the correlated energy spread out of the gun. When compared with simulation, the correlation agrees qualitatively with the measured 0-mode. The simulation gives 11.8% for the 0-mode field relative to the π-mode; this is to be compared with the RF probe measurement of an S-band gun which indicated 3-5%.

Simulations were performed to determine how large a mode separation was needed were performed for an S-band gun. The studies used field maps for the 0- and π-modes generated by the SUPERFISH code [2.16] and the electron dynamics was simulated in PARMELA [2.33]. The case for 1 nC was optimized up to a beam energy of 135 MeV and the sensitivity to the difference between the 0- and π-modes determined for separation frequencies of 3.5 MHz and 15 MHz with 10% and 3% expected field strength compared to the π-mode field, respectively [2.34]. A reasonable metric is the tolerance of the emittance to the phase difference, therefore choose the range of 0-π phase, for which the normalized projected emittance is under 1 μm for a bunch charge of 1 nC. The simulations for 3.5 MHz and 10% field give ~10˚ S phase range. The 15 MHz and 3% 0-mode field has an emittance < 1 μm over the 70˚ S of phase studied. Interestingly enough, the optimum emittance for the 15 MHz cavity shape for the π-mode, but with no 0-mode field had lower emittance than did the 3.5 MHz cavity shape without a 0-mode. The difference in emittance is only 5% but suggests the beam dynamics appear to prefer the large mode separation.

2.5 SOLENOIDS, WAKEFIELD MITIGATION AND DIAGNOSTICS

This section discusses the gun solenoids used for focusing the beam out of the gun and cancelling any fringe fields there may be at the cathode. The section also will cover the major components in the beamline between the gun and the first accelerator. This beamline will be referred to as the Gun-To-Linac (GTL).

2.5.1 The Emittance Compensation Solenoid

As discussed in Chapter 1, the strong defocusing of the beam by the gun's RF requires compensating with an equally strong focusing lens. This focusing lens is usually an electromagnetic solenoid, which may or may not have iron to increase the axial field. Also discussed in Chapter 1 are the effects this solenoid can have on the beam emittance. The first and most important phenomenon is that of emittance compensation, in which the lens focuses the plasma oscillation of the slices to align them to minimize the projected emittance. Emittance compensation was described in Section 1.4.4. In addition, there are the aberration effects of the "perfect" solenoid. These included the chromatic and geometric aberrations, as well as the anomalous quadrupole emittance.

The discussion of the gun solenoid in Section 1.1.5 provides the general requirements for the engineering of the gun's solenoid. To facilitate the present discussion, the solenoid used in the LCLS gun will be used as an example. This solenoid is very similar to that used in the BNL/SLAC/UCLA S-band gun, with the addition of the quadrupole correctors described earlier in Section 1.5.4.

The LCLS gun solenoid consists of eight pancake coils wound from hollow, square copper tubing. In each pancake, the tubing is wound continuously from the outside to the inside to form two layers. Between the pancake coils are iron plates which concentrate and straighten the magnetic flux to give a more uniform magnetic field. There are also thin, iron mirror plates on the ends to contain the fringe fields. The potted coils and iron plates are stacked on a support tube and clamped together to form the solenoid assembly. Also, it is important that all the ends of the pancake coils exit along one side the solenoid and are kept close to each other to cancel fields due to the current in the ends of the conductors. An engineering drawing of the solenoid is shown in Figure **2.14**. Further design details can be found in [2.35].

An interesting feature of the LCLS solenoid design is the inclusion of quadrupole correctors. Inside the solenoid, running its full length, are the normal and skew quadrupole correctors. Each consists of a single run of 16 AWG enameled wire running down the solenoid, across a quarter the circumference of the bore, then back again to form the four poles of a quadrupole. The two correctors on their ~3.3" diameter support spool are shown in Figure **2.15**. This spool fits inside the solenoid's bore as indicated in Figure **2.15** and

Figure **2.18**, where one can see the four electrical leads extending from the beam exit end of the solenoid. At 12 A, each corrector has a focal length of 20 m. During beam operation, the 12 A was to be increased to 15 A to minimize the emittance, thus future uses of this concept should roughly double this corrector integrated field strength of 15 G. Clearly, the power supplies for these correctors should be bi-polar.

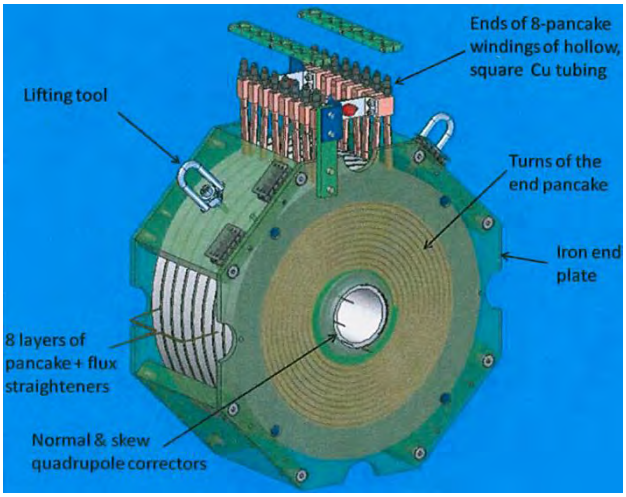

Figure 2.14. Engineering drawing of the LCLS gun solenoid. [2.35]

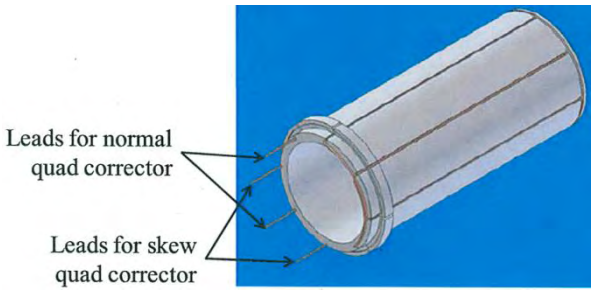

Figure 2.15. Drawing of the 4-wire wire normal and skew quadrupole correctors for the LCLS gun solenoid. [2.35]

In addition to the quadrupole correctors, there are horizontal and vertical steering coils placed on the beam tube inside the solenoid. These coils are capable of steering the 6 MeV beam 20 milliradians with a current of 10 A, and are shown in Figure **2.16**. While useful, it was found during beam commissioning that these steering coils produce oddly shaped beams due to the rotation in the solenoid, and in practice seldom used. Instead, the steering should be done with coils located immediately after the solenoid.

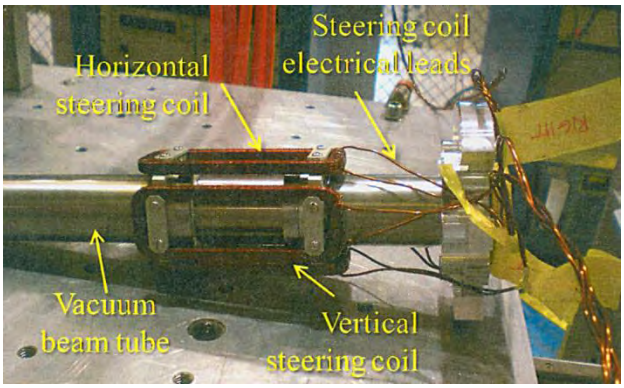

Figure 2.16. Photograph of the dipole steering coils for the LCLS gun. These steering coils are attached to the beam tube which will be installed inside the bore of the gun solenoid.

To achieve the best possible beam quality the gun system also requires a coil to cancel or "buck out" the fringe field from the gun solenoid at the cathodes. Any longitudinal magnetic field at the cathode will cause the electron beam to have an angular momentum about its longitudinal axis. This angular momentum is conserved as described by Busch's theorem [2.36]. Such a magnetized beam has an emittance given by [2.37].

$$\varepsilon_N = \frac{eB_z r_0^2}{8mc} \tag{2.20}$$

This expression gives 0.07 μm for a magnetic field of 10 G and a beam radius of 1 mm. The black bucking coil is seen in Figure **2.17** during characterization in the SLAC magnetic measurements lab.

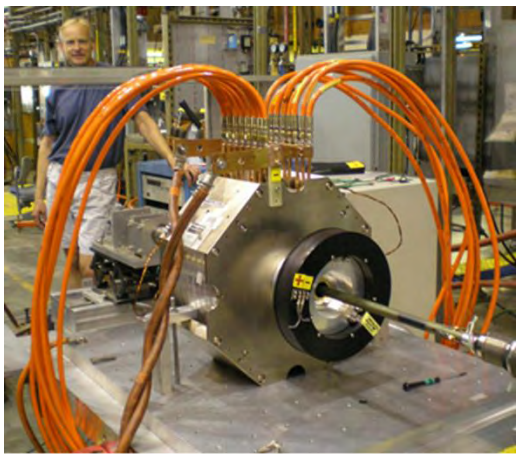

Figure 2.17. The emittance compensation solenoid and bucking coil in the SLAC magnetic measurements lab. [2.19]

Extensive magnetic measurements were made of the gun solenoid fields because of their critical role in compensation of the space charge emittance. Figure **2.18** shows these measurements for the LCLS gun solenoid. At the top of the figure is the Hall probe data for the axial field. This data gives the interior field calibration as a function of the current, shows any hysteresis effects, and provides the effective length of the solenoid. The measured field map is used in the beam simulations. The lower portion of Figure **2.18** gives the quadrupole field measured with a short (2.5 cm long) rotating coil. This type of coil gives the magnetic multipoles as a function of position along the solenoid. This device gives the field magnitude and the multipole phase at the radius of the coil. The phase angle is defined such that 0˚ corresponds to a skewed quadrupole and 90˚ corresponds to a normal quadrupole orientation.

The effects the solenoid quadrupole fields have on the beam have been discussed in some detail in Chapter 1, Section 1.5.4. As a reminder, they are the principle cause of the coupling between the *x*- and *y*-phase spaces, thus increasing trace space emittance. Since the canonical emittance is unaffected, the trace space emittance is fully recoverable using small normal and skewed corrector quadrupoles. The long corrector quadrupoles for the LCLS gun described above (see Figure **2.15**) were installed inside the solenoid's bore as shown in the photographs of Figure **2.19**. For the section of the backup LCLS gun, there are short printed circuit board quadrupoles (PCquads) mounted inside and at each end of the solenoid's bore. As shown in Figure **2.20**, these short quadrupoles are more effective at local cancelation of the anomalous quadrupole field than are the long, corrector quadrupoles. However, local cancellation is not necessary since the theory presented in Chapter 1, Section 1.5.4 shows that a pair of normal and skewed quadrupoles located anywhere near the solenoid can recover the trace space emittance.

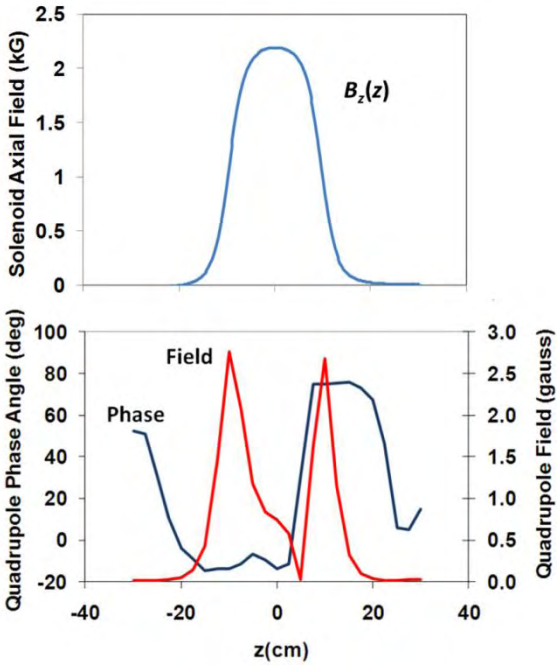

Figure 2.18. Top: Hall probe field map of the LCS gun solenoid along the beam axis. Bottom: A short rotating coil measurement of the quadrupole field magnitude and phase angle. The short coil radius is 2.86 cm and has a length of 2.5 cm.

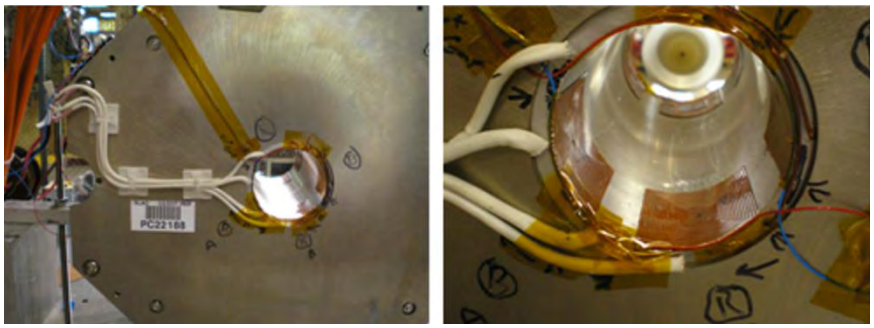

Figure 2.19. Photographs showing the solenoid for Gun–2 showing the single wire and PC quadrupole correctors. The rotating coil used for measuring the field multipoles can be seen at the far end of the solenoid bore. [2.19]

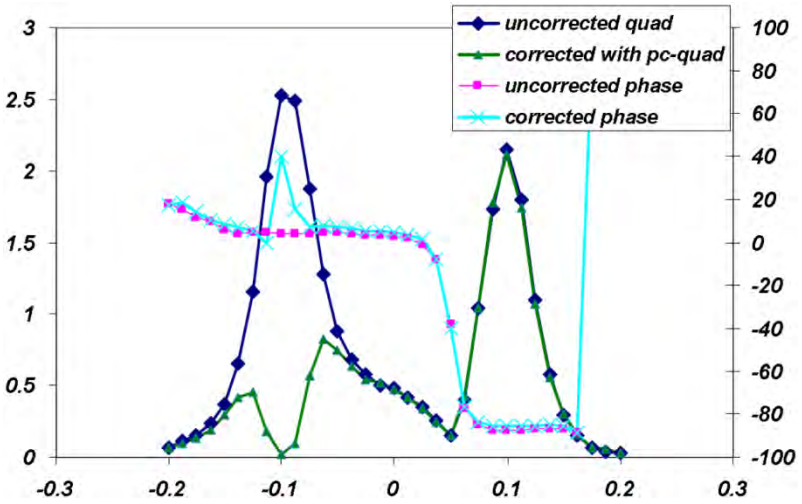

Figure 2.20. Rotating coil measurements of the quadrupole field and phase along the solenoid's magnetic axis showing the uncorrected and corrected anomalous quadrupole field. The correction has been made only for the quadrupole field at the z = -0.1m end of the solenoid. The field at z = 0.1 m is uncorrected. [2.19]

2.5.2 Wakefield Mitigation and Diagnostics in the Gun-to-Linac Beamline

The distance between the gun and the first linac section is determined by emittance compensation; it is ~1-2 m, depending upon the details of the gun voltage and solenoid configuration. A combination of diagnostics and the laser injection optics (for near-normal laser injection) need to fit into this region. For high bunch charge operation, it is important to design the beam pipe vacuum crosses and other vacuum chambers with wakefield liners allowing the beam a smooth and continuous boundary. The wakefield mitigation is even more critical for high duty guns, where the wake due to the preceding bunch can affect the subsequent bunches. As a design philosophy, one usually ignores longitudinal wakes as they can be compensated for by a small phase change of the beam relative to the linac section. On the other hand, it is more important to mitigate transverse wakes since they directly affect the emittance and are more difficult to correct later in the beam line.

Figure **2.21** shows a cutaway view of the GTL region built for the LCLS injector. This design includes dual laser in-vacuum metal mirrors, three Ce:YAG view screens, current toroid, three beam position monitors and an electron spectrometer. All these components have wakefield mitigation liners for the diagnostic and spectrometer vacuum chamber. A custom, all-metal valve was used after the solenoid to isolate the gun from the GTL. When this valve closes, it inserts a tube the same diameter as the vacuum pipe.

The dual laser mirrors on opposite sides of the beam balance the transverse wakes. These mirrors are all-metal to avoid electrostatic charging by low energy electrons and for high damage threshold. The mirror construction is Ni plating onto a BeCu substrate [2.38]. The surface flatness is $\lambda/10$ with a scratch and dig of 15-10. The surface roughness was less than 20 Å rms or 2×10^{-9} m rms.

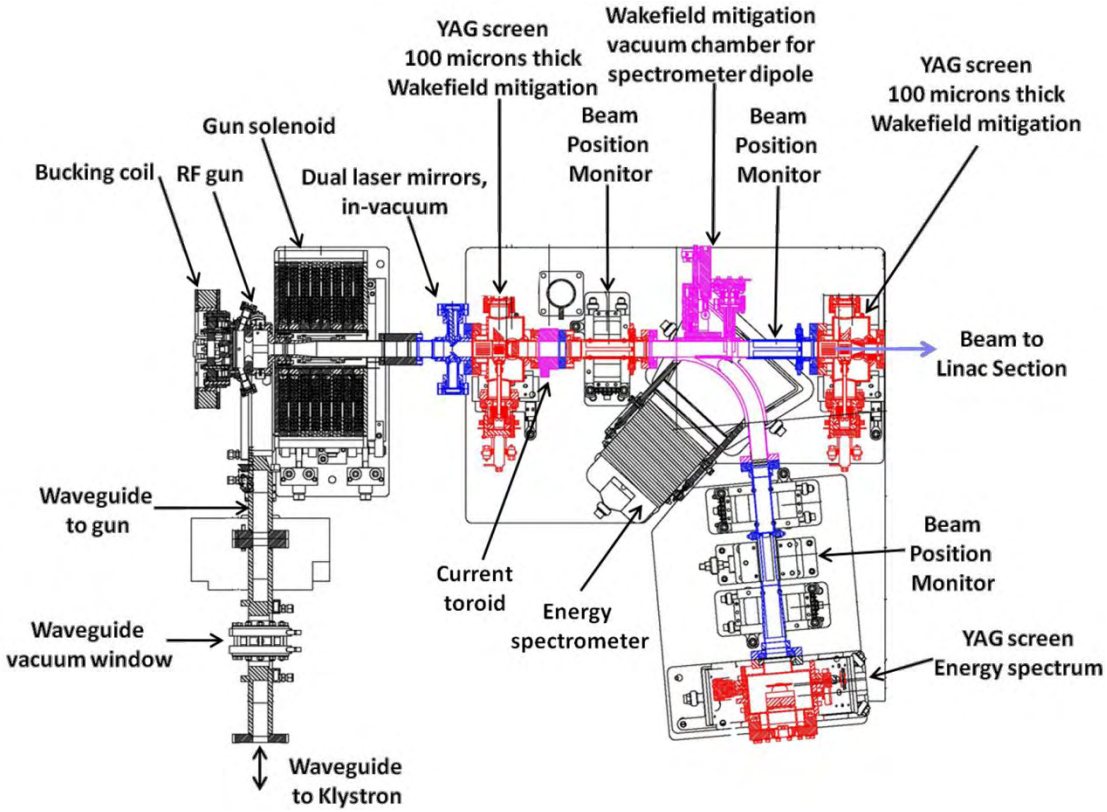

Figure 2.21. Cutaway view of the LCLS Gun-to-Linac region. The overall length of the beam line including the gun is approximately 1.5 m. See [2.39] for more details.

The Ce:YAG view screens were 100 μm thick and mounted normal to the beam. A 45˚ metal mirror behind reflects the fluorescent light from Ce:YAG through a quartz window to the digital camera. When these screens are retracted, the wakefield is mitigated by a cylindrical tube which gives a continuous wall, as seen by the beam. These tubes have longitudinal slots to increase the vacuum conductance to the arms of the cross. There is no electrical or RF connection between the wakefield plug and the beam tube. Instead, the length of the gap between the beam tube and plug was designed to be much less than a bunch length, which for 10 ps is 3 mm FWHM.

Although the space is limited, a dipole magnetic spectrometer was built for the LCLS GTL. This 85˚ dipole images the beam from the first YAG to the focal plane of the spectrometer in both the horizontal and vertical planes. The magnet requires a small trim coil for cancelling the remnant magnetic field. Equally important is determining a reproducible procedure for setting and cancelling this magnets field. The dipole magnet vacuum chamber also is wakefield mitigated for the straight through beam path. The mitigation is done with a plate which conforms to and covers the opening to the spectrometer.

2.6 EXAMPLES OF NCRF GUNS

2.6.1 Low Duty Factor Guns

LANL 5½-Cell L-Band Gun

Based on the experience gained in building the first photocathode RF gun, LANL designed and operated a 1.3 GHz (L-band) gun with 5½-cells as shown in Figure **2.22** [2.7].

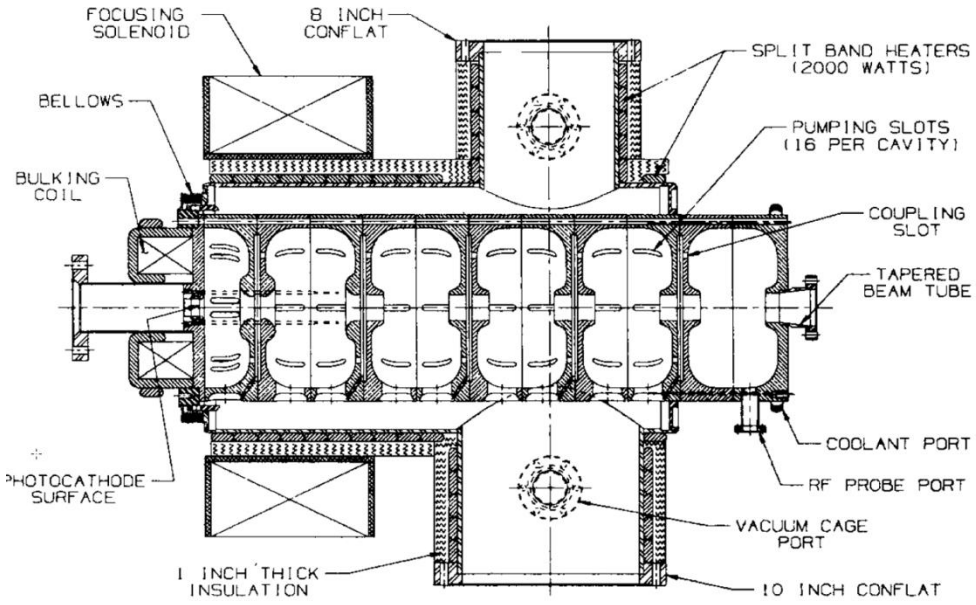

Figure 2.22. The LANL 5½-cell RF gun with compensation solenoid and bucking coil. [Reprinted from [2.7], with permission from Elsevier.]

This gun was built in the early days of emittance compensation, before it was realized that the beam quality is further improved if the first cell is extended from a 0.5 cell length to 0.6 long (0.6*λ/2). The gun Q_0 was 18 500 and the shunt impedance 53 MΩ m^{-1}. The gun operated at 0.1% duty factor requiring 2.4 MW of RF power to produce a 0.6 MW beam. The cell-to-cell RF fields are not balanced in this gun and average accelerating fields were 26 MV m^{-1}, 14 MV m^{-1} and 10 MV m^{-1} for cell 1 (cathode cell), 2 and 3, respectively. The gun was built with vacuum pumping preeminently in mind. The cavities were held inside a vacuum can. Slots in the cavities gave extra pumping of all the cavities into the common vacuum plenum.

The gun was used in several successful FEL experiments, most noteworthy being the regenerative amplifier FEL [2.40].

CEA 144 MHz Gun

At the low end of the RF frequency scale is the 144 MHz gun cell built and operated by the CEA facility at Breyères Le Châtel, France. A drawing of the gun and the test beam line is shown in Figure **2.23**. The RF structure used reentrant nose cones to boost the cathode field to 25 MV m^{-1} and accelerate the beam in a single gap to ~1.5 MeV. A goal of this gun was to produce a long train of high charge bunches which are further accelerated and used to power an FEL. One operating mode was 2 nC bunches at 72 MHz giving an average current of 144 mA during a 200 μs macropulse. This remains a difficult goal to achieve, even given today's technology, with the cathode lifetime severely limiting the operating time. The first version of this gun had a very short cathode 1/*e* lifetime of only 15 min. Therefore, a second gun was built with a much better vacuum. In 2002, the new gun demonstrated 1 μm emittance for a 1 nC bunch charge, which is a difficult emittance to achieve at any frequency. The bunch length was 60 ps making the peak current ~17 A. [2.41]

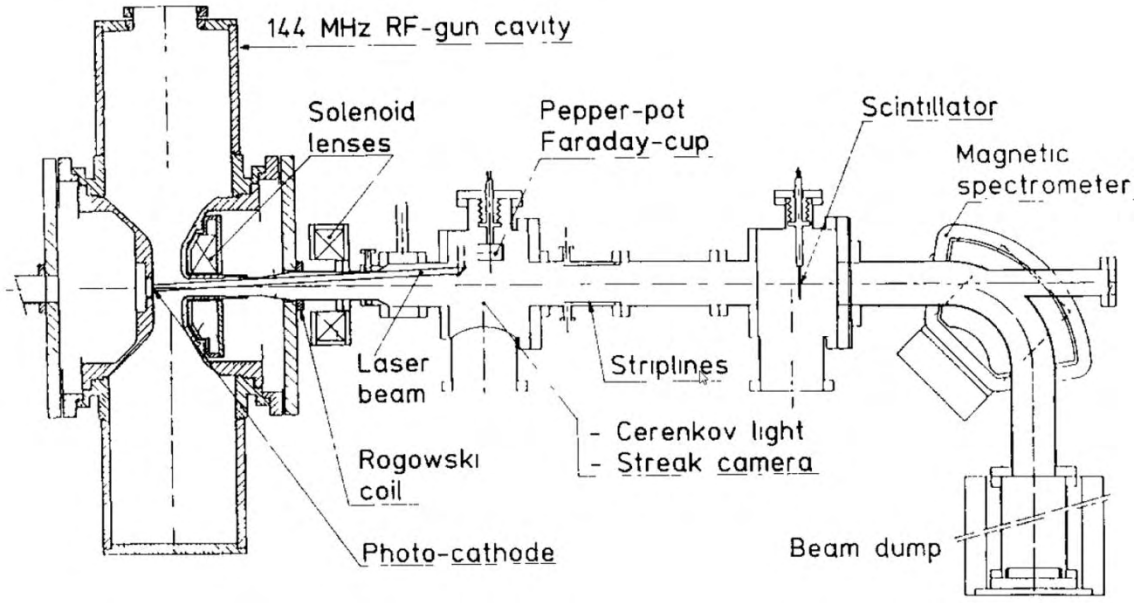

Figure 2.23. CEA 144 MHz RF gun and beam line to first accelerator section [2.3]. [Reprinted from [2.42], with permission from Elsevier.]

The BNL, BNL/SLAC/UCLA, LCLS S-band guns

In 1988, McDonald published a paper describing a pillbox S-band gun for the BNL Accelerator Test Facility (ATF) to provide electron beams for research on laser acceleration, inverse FEL's and nonlinear Compton scattering [2.43]. McDonald's paper is remarkable for all the things it reported on correctly, while missing other major factors. It described in detail the performance of a high field RF gun and was the first to quantify the RF and space charge emittances. This was done both numerically and analytically. Appendix A in [2.43] presents an interesting analysis of the radial RF fields and describes a cavity shape which minimizes the nonlinear components of these fields. But, what's missing is the gun solenoid: the paper never mentions the solenoid and its critical role in emittance compensation.

Four years later, in 1992, the Linac Coherent Light Source (LCLS) was proposed by Claudio Pellegrini and a collaboration of SLAC, Brookhaven and UCLA was formed to develop the gun. McDonald's gun became

the obvious first choice for LCLS gun since it was at the same S-band frequency as the SLAC linac and simulations showed it could deliver the LCLS beam brightness. This led to the birth of the BNL/SLAC/UCLA S-band gun.

The BNL/SLAC/UCLA gun proved to be successful in the sense of being replicated in several labs and universities. In the end, it also was successful in its original goal of investigating how to make the bright beam required for LCLS and other FEL projects. Beam studies of the BNL/SLAC/UCLA gun showed what was limiting its performance and how to remove these limitations in the LCLS gun design.

The DESY/PITZ Gun

The DESY/PITZ gun is the first gun designed with symmetric RF fields and the first gun to use a coaxial feed for the RF power. This innovative pillbox L-band gun is illustrated in Figure **2.24**, which also shows the cathode transfer system and beamline downstream of the gun.

The coaxial feed gun has complete rotational symmetry, since there are no penetrations for laser ports or for RF probes. This simplifies the engineering design and avoids the problems of heating around the penetrations as discussed above. Another advantage of not having any ports or probes is this allows greater flexibility in placing the solenoid close to the cathode to maintain a small electron beam size. This advantage has been fully optimized in the S-band version.[2.44]

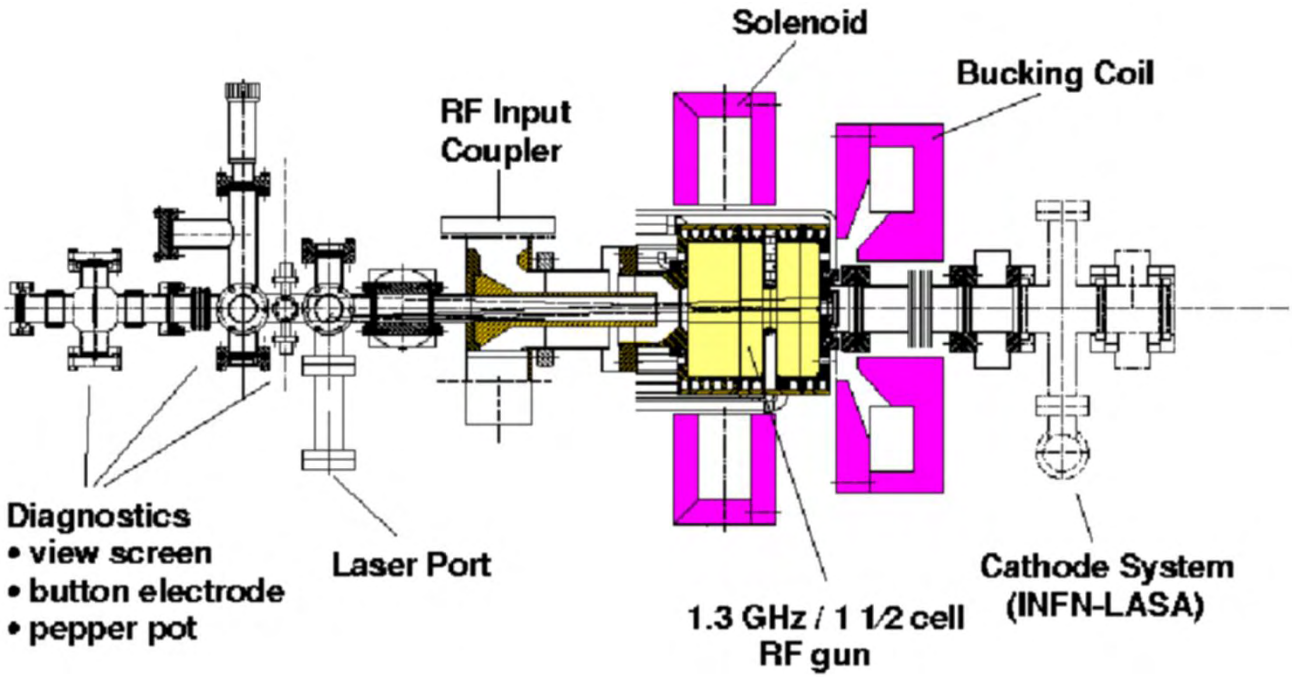

Figure 2.24. The DESY/PITZ coaxial feed gun. [Courtesy of F. Stephan (DESY/PITZ)]

However, there remain a few potential disadvantages of the coaxial feed. The first is the center conductor tube of the coax feed needs to be precisely positioned with respect to the gun cell. The coaxial is a low field region and low RF field regions are often susceptible to multipacting; this does not appear to be an issue since there is no evidence of multipacting during operation of the DESY/PITZ gun. And as an issue concerning RF controls, no penetrations means not having RF probe signals for the LLRF controls (see Section 2.3.2). Although the forward and reverse power can be used for RF controls, gun probes provide a direct measure of the cavity fields and are useful for at least the prototype version of the gun. Calculations

and experience show that the field perturbation and heating around the probe port are small effects, but care is needed in locating the probe to avoid mechanical interference with the solenoid.

The DESY/PITZ gun was developed for the European X-ray Free Electron Laser and has successfully demonstrated sub-micron emittance at 1 nC which is required for that project [2.45], [2.46]. In addition this gun is capable of operating at 1% duty factor with 1 ms long RF macropulses at 10 Hz repetition rate. There can be up to 8 000 1 nC bunches per 1 ms long macropulse. The gun Q_0 is 21 500 and the peak cathode field is 40-60 MV m^{-1}.

2.6.2 High Duty Factor Guns

The Boeing/LANL 433 MHz Gun

Seven years after the first electrons were accelerated from a photocathode, a high duty factor gun demonstrated an average current of 32 mA in a 25% duty factor system. This giant leap of three orders of magnitude in duty factor was made possible due to aggressive funding by the Strategic Defense Initiative from 1983 to 1992. The electron gun was a 25% duty factor prototype of the CW electron source for a defensive free electron laser.

The gun consisted of two independently powered (and phased) reentrant cavities operating at 433 MHz. The waveguides for the two cavities dominate the photograph insert of Figure **2.25**. The accelerator and photocathode configuration used in the beam tests is shown in drawing. The beam energy out of the gun was 1.8 MeV with a peak cathode field of 26 MV m^{-1}. The beam was further accelerated to 5 MeV by two more independently powered 433 MHz cavities as shown in the figure. The 25% RF duty factor was produced with 8.3 ms long macropulses at a 30 Hz repetition rate and required 600 kW average RF power to produce the 26 MV m^{-1} cathode field and 1.8 MeV beam. The bunch micropulse frequency was 27 MHz and with bunch charges from 1-7 nC [2.5]. K_2CsSb cathodes were fabricated in a deposition chamber located behind the gun. QEs of 12% at 527 nm laser wavelength were obtained with this system. [2.47]

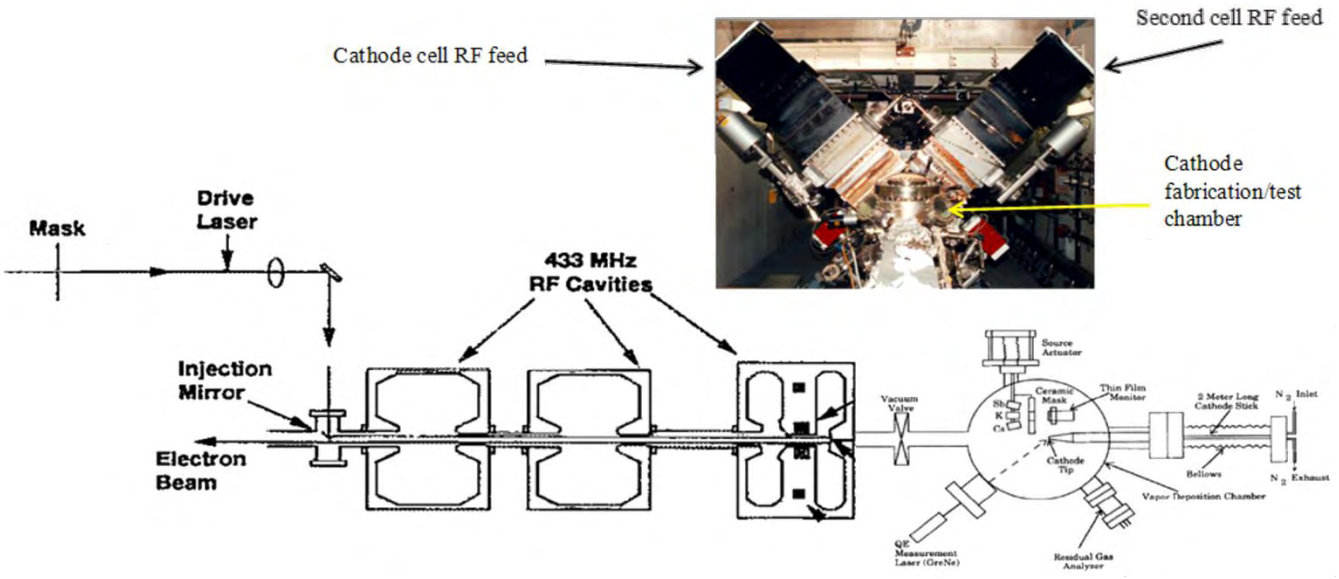

Figure 2.25. Configuration of the 433 MHz high duty factor accelerator and cathode system. Insert: Photograph taken from the photocathode preparation chamber side (rear) of the gun. [Adapted from [2.48], with permission from Elsevier.] [Adapted with permission from [2.5]. Copyright 1993, American Institute of Physics.] [Adapted from [2.47], with permission from Elsevier.]

The LANL/AES 700 MHz Gun

A truly CW NCRF gun is the 700 MHz gun designed by Los Alamos and built by Advanced Energy Systems, Inc. (AES). The unique RF coupler for this gun has been described earlier in this chapter and the full gun configuration is shown in Figure **2.26**. The gun has three cavities with accelerating fields of 7 MV m^{-1}, 7 MV m^{-1} and 5 MV m^{-1} for the cathode and second and third cavities, respectively. The low fields are required to manage the heat load and thermal stresses caused by the high dissipated power. Many of these issues were discussed earlier in the section on RF couplers. The gun has a dummy (unpowered) exit cavity functioning as a vacuum plenum with an array of eight vacuum pumps. The gun has been fabricated and is currently undergoing high power RF testing at LANL.

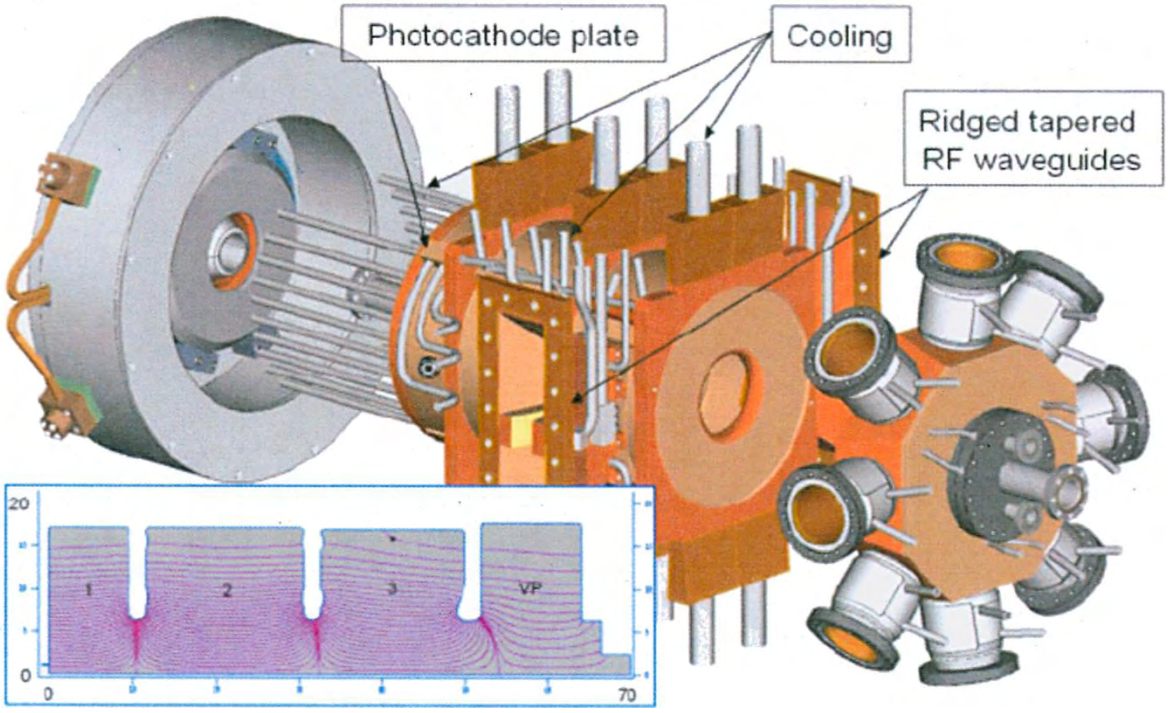

Figure 2.26. The LANL/AES 700 MHz CW RF photocathode gun. [[2.6]; Available under Creative Common Attribution 3.0 License (www.creativecommons.org/licenses/by/3.0/us/) at www.JACoW.org.]

LBNL VHF Gun

The LBNL VHF gun is at the low frequency of 187 MHz to allow CW operation. The gun was designed to have a very good vacuum. As shown earlier in Figure **2.6**, the 187 MHz gun has a row of 104 slots circling the circumference of the cavity. The outer plenum contains a battery of 24 NEG vacuum pumps with a CO pumping speed of 180 L s^{-1} each, or 4 300 L s^{-1} total. This immense pumping speed is necessary to reach the goal of 5×10^{-11} Torr or 6.6×10^{-9} Pa when operating a full CW power. This excellent vacuum is intended to give very long cathode lifetimes.

The gun is a reentrant single-cell cavity with a 40 mm accelerating gap. The cavity Q_0 is 30 877 and the shunt impedance is 6.5 MΩ. The cathode electric field is 19.5 MV m^{-1} and produces a 0.75 MV gap voltage. At this low RF frequency, the electric field appears to be DC for a picosecond long electron bunch. Therefore, effects due to the time-dependence of the RF field, such as the RF emittance, will be small. The peak wall power density is a reasonable 25 W cm^{-2} [2.21].

2.7 SUMMARY

This chapter reviewed the design options for RF guns which are seen to range over the entire RF spectrum. Generally, frequency and duty factor are related. Due to power dissipation limitations, the lower frequency guns are capable of higher duty factors than those of high frequencies. The maximum achievable field scales with the RF frequency, with the field limit given by the Kilpatrick criterion. Experience shows that operational fields with "bravery" factors of two and more times the Kilpatrick criterion is possible. The two cavity shape options are the pillbox and reentrant. The pillbox is easily fabricated and is generally used at high RF frequencies. The reentrant shape is more common at low frequencies and has higher on-axis field than the pillbox for the same RF power.

After reviewing the basics of RF gun theory, the two methods for coupling the RF power into the gun were discussed. These are side coupling and coaxial coupling. For the more commonly used side coupling, the RF power enters through a port hole located in the side of the cavity. For guns with multiple cavities, the power then flows into the other cavities through the irises between the cavities, or through slots in the walls between the cavities. The major disadvantages of side coupling are local heating by average and pulsed heating around the edge of the port, and the introduction of field asymmetries. The field asymmetries can be corrected using dual feeds and a racetrack shape of the coupling cavity. In addition, the waveguide's location protruding from the side of the cavity limits the options for placement of the solenoid. In coaxial coupling, the RF power is brought into the gun on the cavity's axis using a "door-knob" transition which converts the rectangular waveguide mode into an on-axis coaxial mode. The RF power fills the gun through the cavity irises. The advantages of coaxial coupling are the absence of penetrations in the cavity walls and their induced local heating and a symmetric field without the need for specialized cavity shapes. The solenoid can be placed much closer to the cathode, since the door-knob coupler is now downstream of the gun. A disadvantage is the possibility of multipacting in the low field regions of the center conductor.

Examples of two high performance guns are described in some detail: One operating at low duty factor and high field, and the other designed for high duty factor and low field. The low duty factor, high field gun was designed for an X-ray Free Electron Laser (FEL). The high field was essential to get the high brightness needed for the SASE FEL. The high duty factor, low field gun is intended for use in a CW FEL operating at IR wavelengths. In each case, the RF coupler issues dominate the design.

The RF power system is briefly described illustrating the need for control loops on both the low level RF and the cooling water to maintain the gun's resonant frequency. This is followed by sections discussing the emittance due to asymmetric RF fields and solenoid effects in a working gun. The theory is given in Chapter 1.

Wake field mitigation and electron beam diagnostics in the gun-to-linac region is then briefly reviewed. The mitigation of the beam view screens is described in more detail in Chapter 10. Here, the added feature of shielding the spectrometer vacuum chamber is discussed.

The chapter finishes with a short descriptions and comments on examples of low- and high-duty factor RF guns built since the invention of the photoinjector. The low duty factor guns are represented by the LANL 5½-cell 1 300 MHz gun, the CEA 144 MHz gun, the BNL S-band gun and the DESY-PITZ L-band gun. The high-duty factor guns are the Boeing/LANL 433 MHz gun, the LANL 700 MHz gun and the LBNL VHF gun.

The intent of this chapter was to introduce the reader to the rich diversity of the NCRF guns which span nearly the entire range of RF frequency and operational duty factor. It is hoped that this short introduction educates new practitioners of this dynamic field and becomes a useful reference for the experts as they continue to advance the technology of NCRF photoinjectors and electron sources in general.

2.8 CONFLICT OF INTEREST AND ACKNOWLEDGEMENTS

The author confirms that this article content has no conflicts of interest.

References

[2.1] W. D. Kilpatrick, "Criterion for vacuum sparking designed to include both RF and DC," *Rev. Sci. Instrum.*, vol. 28, pp. 824-826, October 1957.

[2.2] T. Wangler, *RF Linear Accelerators*, Weinheim: Wiley-VCH Verlag, 199, pp. 1608.

[2.3] S. Joly, P. Balleyguier, Cl. Bonetti *et al.*, "Progress report on the BRC photo-injector," in *Proc. 1990 European Particle Accelerator Conf.*, 1990, pp. 140-142.

[2.4] J. W. Staples, K. M. Baptiste, J. N. Corlett *et al.*, "Design of a vhf-band rf photoinjector with megahertz beam repetition rate," in *Proc. 2007 Particle Accelerator Conf.*, 2007, pp. 2990-2992

[2.5] D. H. Dowell, K. J. Davis, K. D. Friddell *et al.*, "First operation of a photocathode radio frequency gun injector at high duty factor," *Appl. Physics Lett.*, vol. 63, pp. 2035-2037, October 1993.

[2.6] S. S. Kurennoy, D. C. Nguyen, D. L. Schrage *et al.*, "Normal-conducting high current RF photoinjector for high power cw FEL," in *Proc. 2005 Particle Accelerator Conf.*, 2005, pp. 2866-2868.

[2.7] L. M. Young, "Compact photoinjector accelerators for free electron lasers," *Nucl. Instrum. Meth. B*, vol. 56-57, pp. 978-981, May 1991.

[2.8] R. Bakker, M. v. Hartrott, E. Jaeschke *et al.*, "First measurements at the photo injector test facility at DESY ZEUTHEN," in *Proc. 2002 European Particle Accelerator Conf.*, 2002, pp. 1813-1815.

[2.9] L. Xiao, R. F. Boyce, D. H. Dowell *et al.*, "Dual feed RF gun design for the LCLS," in *Proc. 2005 Particle Accelerator Conf.*, 2005, pp. 3432-3434.

[2.10] A. E. Vlieks, V. Dolgashev, S. Tantawi *et al.*, "X-band RF gun development," in *Proc. 2010 Int. Particle Accelerator Conf.*, 2010, pp. 3816-3818.

[2.11] A. S. Kesar, J. Haimson, S. Korbly *et al.*, "Initial testing of a field symmetrized dual feed 2 MeV 17 GHz RF gun," in *Proc. 2003 Particle Accelerator Conf.*, 2003, pp. 2095-2097.

[2.12] A. Brinkmann, D. Reschke and J. Ziegler, "Various applications of dry-ice in the field of accelerator components at DESY," in *Proc. 2008 Linear Accelerator Conf.*, 2008, pp. 803-805.

[2.13] F. Stephan, J. W. Bähr, C. H. Boulware *et al.*, "New experimental results from PITZ," in *Proc. 2008 Linear Accelerator Conf.*, 2008, pp. 474-476.

[2.14] J. W. Staples, S. M. Lidia, S. P. Virostek *et al.*, "The LBNL femtosource (LUX) 10 KHz photoinjector," in *Proc. 2003 Particle Accelerator Conf.*, 2003, pp. 2092-2094.

[2.15] J. D. Jackson, *Classical Electrodynamics*, 3rd Ed., New York: Wiley, 1999, pp. 373.

[2.16] J. H. Billen and L. M. Young, "Poisson SUPERFISH," Los Alamos National Laboratory, Technical Report LA-UR-96-1834, updated 2003.

[2.17] T. Wangler, *RF Linear Accelerators*, Weinheim: Wiley-VCH Verlag, 1998, pp. 141-144.

[2.18] J. Haimson, B. Mecklenburg and E. L. Wright, "A racetrack geometry to avoid undesirable azimuthal variations of the electric field gradient in high power coupling cavities for TW structures," in *Proc.AIP Conf.*, vol. 398, pp. 898-911, March 1997.

[2.19] D. H. Dowell, E. Jongewaard, J. Lewandowski *et al.*, "The Development of the Linac Coherent Light Source RF Gun," LCLS, Stanford, California, Technical Report No. SLAC PUB-13401, September 2008.

[2.20] B. Dwersteg, K. Flöettmann, J. Sekutowicz *et al.*, "RF gun design for the TESLA VUV free electron laser," *Nucl. Instrum. Meth. A*, vol. 393, pp. 93-95, July 1997.

[2.21] K. Baptiste, J. Corlett, R. Kraft *et al.*, "Status and plans for the LBNL normal-conducting cw vhf photo-injector," in *Proc. 2009 Free Electron Laser*, 2009, pp. 470-472.

[2.22] P. Pritzkau and R. H. Siemann, "Experimental study of RF pulsed heating on oxygen free electronic copper," *Phys. Rev. ST Accel. Beams*, vol. 5, pp. 112002-1–112002-22, November 2002.

[2.23] D. H. Dowell, L. Bentson, R. F. Boyce *et al.*, "RF design for the linac coherent light source (LCLS) injector," in *Proc. 2004 Free Electron Laser Conf.*, 2004, pp. 538-541.

[2.24] R. Boyce, D. H. Dowell, J. Hodgson *et al.*, "Design considerations for the LCLS RF gun," LCLS, Stanford, California, Technical Report No. LCLS-TN-04-4, April 2004.

[2.25] S. S. Kurennoy, D. L. Schrage, R. L. Wood *et al.*, "Photoinjector RF cavity design for high power CW FEL," in *Proc. 2003 Particle Accelerator Conf.*, 2003, pp. 920-922.

[2.26] S. S. Kurennoy and L. M. Young, "RF coupler for high-power CW FEL photoinjector," in *Proc. 2003 Particle Accelerator Conf.*, 2003, pp. 3515-3517.

[2.27] L. M. Young, D. E. Rees, L. J. Rybarcyk *et al.*, "High power RF conditioning of the LEDA RFQ," in *Proc. 1999 Particle Accelerator Conf.*, 1999, pp. 881-883.

[2.28] MicroWave Studio, ver. 4.2, available by Computer Simulation Technology GmbH, Bad Nauheimer Str. 19, 64289 Darmstadt, Germany. Available at www.cst.com/Content/Products/MWS/Overview.aspx.

[2.29] SCM Metal Products, http://en.wikipedia.org/wiki/Glidcop.

[2.30] Z. Li, N. Folwell, L. Ge *et al.*, "High performance computing in accelerator structure design and analysis," in *Proc. 2004 Int. Computational Accelerator Physics*, 2004.

[2.31] Z. Li, J. Chan, L. D. Bentson *et al.*, "Coupler design for the LCLS injector s-band structures," in *Proc. 2005 Particle Accelerator Conf.*, 2005, pp. 2176-2178.

[2.32] J. F. Schmerge, J. Castro, J. E. Clendenin *et al.*, "The s-band 1.6 cell RF gun correlated energy spread dependence on π and 0 mode relative amplitude," in *Proc. 46th Physics Applications High Brightness Electron Beams Workshop*, 2005, pp. 375-382.

[2.33] L. M. Young, "PARMELA documentation," Los Alamos National Laboratory, Los Alamos, NM, Technical Report No. LA-UR-96-1835 (Revised June 8, 2004).

[2.34] C. Limborg, Z. Li, L. Xiao *et al.*, "RF Design of the LCLS Gun," LCLS, Stanford, California, Technical Report No. LCLS-TN-05-3, February 2005.

[2.35] J. Schmerge, "LCLS gun solenoid design considerations," LCLS, Stanford, California, Technical Report No. LCLS-TN-05-14, June 2005.

[2.36] M. Reiser, *Theory and Design of Charged Particle Beams*, 1st Ed., Weinheim: Wiley-VCH Verlag, 1994, pp. 313.

[2.37] S. M. Gierman, *Streak Camera Enhanced Quadrupole Scan Technique for Characterizing the Temporal Dependence of the Trace Space Distribution of a Photoinjector Electron Distribution*, Ph.D. Thesis, University of California, San Diego, CA, 1999, Appendix C.

[2.38] S. Gilevich, private communication.

[2.39] R. Akre, D. Dowell, P. Emma *et al.*, "Commissioning of the linac coherent light source," *Phys. Rev. ST Accel. Beams*, vol. 11, pp. 030703-1–030703-20, March 2008.

[2.40] D. C. Nguyen, R. L. Sheffield, C. M. Fortgang *et al.*, "A high-power compact regenerative amplifier FEL," in *Proc. 1997 Particle Accelerator Conf.*, 1997, pp. 897-899.

[2.41] J.-G. Marmouget, A. Binet, Ph. Guimbal *et al.*, "Present performance of the low-emittance, high-bunch charge ELSA photo-injected linac," in *Proc. 2002 European Particle Accelerator Conf.*, 2002, pp. 1795-1797.

[2.42] R. Dei-Cas, P. Balleyguier, J. Bardy *et al*., "Photo-injector, accelerator chain and wiggler development programs for a high peak power rf free electron laser," *Nucl. Instrum. Meth. A*, vol. 285, pp. 320-326, December 1989.

[2.43] K. T. McDonald, "Design of the laser-driven RF electron gun for the BNL accelerator test facility," *Trans. Electron Devices*, vol. 35, pp. 2052-2059, November 1988.

[2.44] J-H. Han, M. Cox, H. Huang *et al.*, "Design of a high repetition rate S-band photocathode gun," *Nucl. Instrum. Meth. A*, vol. 647, pp. 17-24, August 2011.

[2.45] F. Stephan, C. H. Boulware, M. Krasilnikov *et al*., "Detailed characterization of electron sources yielding first demonstration of European X-ray free-electron laser beam quality," *Phys. Rev. ST Accel. Beams*, vol. 13, pp. 020704-1–020704-33, February 2010.

[2.46] S. Rimjaemm, G. Asova, J. Bähr *et al.*, "Measurements of transverse projected emittance for different bunch charges at PITZ," in *Proc. 2010 Free Electron Laser Conf.*, 2010, pp. 410-413.

[2.47] D. H. Dowell, S. Z. Bethel and K. D. Friddell, "Results from the average power laser experiment photocathode injector test," *Nucl. Instrum. Meth. A*, vol. 356, pp. 167-176, March 1995.

[2.48] A. Todd, "State-of-the-art electron guns and injector designs for energy recovery linacs (ERLs)," *Nucl. Instrum. Meth. A*, vol. 557, pp. 36-44, February 2006.